Vortex energy and 360°–Néel wall in thin–film micromagnetics

Radu Ignat *, Hans Knüpfer †

October 26, 2009

Abstract

We study the vortex pattern in ultra-thin ferromagnetic films of circular cross-section. The model is based on the following energy functional:

$$E_\epsilon^{2d}(m) = \epsilon \int_{B^2} |\nabla m|^2 \, dx + \frac{|\ln \epsilon|}{2} \int_{\mathbb{R}^2} \left| |\nabla|^{-1/2} (\nabla \cdot m \, \mathbb{1}_{B^2}) \right|^2 dx,$$

for in–plane magnetizations $m : B^2 \to S^1$ in the unit disc $B^2 \subset \mathbb{R}^2$. The avoidance of volume charges $\nabla \cdot m \neq 0$ in B^2 and surface charges $m \cdot \nu \neq 0$ on ∂B^2 leads to the formation of a vortex in the limit $\epsilon \to 0$. At level $\epsilon > 0$, the vortex is regularized by formation of a 360°–Néel wall (a one-dimensional transition layer with core of scale ϵ) concentrated along a radius of B^2. We derive the limiting energy of the vortex by matching upper and lower bounds. Our analysis on the lower bound is based on a dynamical system argument and an interpolation inequality with sharp leading order constant, while the upper bound uses the leading order energy for 360° Néel walls.

AMS classification: Primary: 49S05, Secondary: 82D40, 35A15, 35B25.
Keywords: singular perturbation, vortex, Néel wall, micromagnetics.

Contents

*Laboratoire de Mathématiques, Université Paris-Sud 11, bât. 425, 91405 Orsay, France (e-mail: Radu.Ignat@math.u-psud.fr)
†Courant Institute, New York University, New York, NY 10012, USA (e-mail: knuepfer@cims.nyu.edu)

1 Introduction & Statement of Results

In thin ferromagnetic films, variations of the magnetization in thickness direction as well as its out of plane component are energetically strongly penalized. This leads to a reduced two–dimensional variational model where the magnetization is described by a two–dimensional unit vector field. The geometry of the sample influences the pattern formation for the magnetization: In the case of a magnetic sample with circular cross-section, we asymptotically expect the formation of a single vortex at the center of the disc. The aim of our paper is to analyze the energetic cost of such a vortex formation.

1.1 The model

We are interested in the energetic cost of a vortex in ultra-thin ferromagnetic films. The analysis is based on the following renormalized two–dimensional micromagnetic energy:

$$E_\epsilon^{2d}(m) = \epsilon \int_{B^2} |\nabla m|^2 \, dx + |\ln \epsilon| \int_{\mathbb{R}^3} |h_{ac}(m)|^2 \, dxdz, \tag{1}$$

where $\epsilon > 0$ is a small parameter. The first term in (1) is called the exchange energy, while the second term stands for the stray field energy created only by the volume charges in the interior of the sample. The model is non–dimensionalized: We assume that the magnetization

$$m : B^2 \to S^1$$

is a unit–length in-plane vector field defined in the unit disc B^2. The stray-field $h_{ac}(m) : \mathbb{R}^3 \to \mathbb{R}^3$ considered here is generated only by the volume charges $(\nabla \cdot m)_{ac} := (\nabla \cdot m)\mathbb{1}_{B^2}$ and is defined as the unique $L^2(\mathbb{R}^3, \mathbb{R}^3)-$gradient field

$$h_{ac}(m) = (\nabla, \frac{\partial}{\partial z}) U_{ac}(m)$$

determined by static Maxwell's equation in the weak sense: For all $\zeta \in C_c^\infty(\mathbb{R}^3)$,

$$\int_{\mathbb{R}^3} (\nabla, \frac{\partial}{\partial z}) U_{ac}(m) \cdot (\nabla, \frac{\partial}{\partial z})\zeta \, dxdz = \int_{B^2} \nabla \cdot m \; \zeta \, dx. \tag{2}$$

Explicitly solving (2) in Fourier space, the stray-field energy can be equivalently expressed in terms of the homogeneous $\dot{H}^{-1/2}-$norm of $(\nabla \cdot m)_{ac}$ (see Appendix):

$$\int_{\mathbb{R}^3} |h_{ac}(m)|^2 \, dxdz = \frac{1}{2} \int_{\mathbb{R}^2} \frac{1}{|\xi|} |\mathcal{F}((\nabla \cdot m)_{ac})(\xi)|^2 \, d\xi = \frac{1}{2} \|(\nabla \cdot m)_{ac}\|^2_{\dot{H}^{-1/2}(\mathbb{R}^2)}. \tag{3}$$

Here and in the following, we denote planar coordinates by $x = (x_1, x_2)$, $(x_1, x_2)^\perp = (-x_2, x_1)$, the vertical coordinate by z and furthermore, we write $(\nabla, \frac{\partial}{\partial z}) = (\frac{\partial}{\partial x_1}, \frac{\partial}{\partial x_2}, \frac{\partial}{\partial z})$.

Essential features of this variational model are the nonconvex constraint $|m| = 1$ and the nonlocality of the stray-field interaction. The competition of exchange energy and stray field energy together with the above constraints leads to a rich pattern formation for stable states of the magnetization. Generically, these patterns consist in large almost uniformly magnetized regions (*magnetic domains*) separated by narrow smooth transition layers (*domain walls*) where the magnetization varies rapidly [11]. The characteristic domain wall observed in ultra thin-films is the Néel wall (corresponding to a one-dimensional in-plane rotation connecting two directions of the magnetization). In particular, we speak about a 360° Néel wall when the magnetization performs a complete turn around a given direction to the wall.

Vortex. Our goal is to analyze the behavior of a vortex configuration. As we shall explain in the following, a vortex in our model is a very peculiar structure that is driven by a 360° Néel wall along a radius of a disc. Therefore, it is a completely different configuration than the Bloch line (a structure characteristic to moderately thick ferromagnetic films, see Section 1.3) or the so called Ginzburg-Landau vortex (characteristic to superconductors).

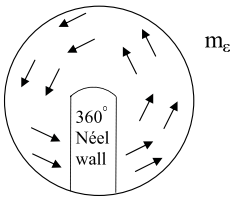

Figure 1: Microscopic vortex structure at level ϵ.

Our viewpoint is based on the method of $\Gamma-$convergence: We enforce the formation of a vortex in the limit $\epsilon \to 0$ by considering families $\{m_\epsilon\}_{\epsilon>0}$ of magnetizations that satisfy

$$m_\epsilon \to \frac{x^\perp}{|x|} \quad \text{in} \quad L^2(B^2) \quad \text{as } \epsilon \to 0. \tag{4}$$

and we define the energy of the vortex by the following relaxed problem:

$$E_0^{2d}(\frac{x^\perp}{|x|}) = \inf \left\{ \liminf_{\epsilon\to 0} E_\epsilon^{2d}(m_\epsilon) \ : \ \{m_\epsilon\} \text{ satisfies (4)} \right\}. \tag{5}$$

Indeed, the infimum in (5) is achieved (and non–trivial). We call a minimizing family, every family $\{m_\epsilon\}$ that satisfies (4) and achieves the minimum (5), i.e. $\lim_{\epsilon\to 0} E_\epsilon^{2d}(m_\epsilon) = E_0^{2d}(\frac{x^\perp}{|x|})$. The L^2-compactness of uniformly bounded energy configurations has been proved in [17] (see also [16] for compactness of magnetizations with values in S^2).

Note that the minimal level of energy E_ϵ^{2d} is trivial and all minima are constant since (1) does not penalize surface charges $m \cdot \nu \neq 0$ on ∂B^2, where ν is the outer normal at ∂B^2. In fact, every finite energy configuration does have surface charges and trivial degree (winding number equal to 0) on each closed curve in B^2. For this reason, both a degree 1 as well as absence of surface charges can only be imposed in the limit $\epsilon \to 0$ (as in (4)). Our analysis shows that asymptotically the vortex state represents the minimum energy E_ϵ^{2d} under the constraint (4). We conjecture that the vortex is still a minimizer if constraint (4) is relaxed and convergence is only assumed on the boundary ∂B^2 (i.e., $m_\epsilon \to x^\perp$ in $L^2(\partial B^2)$ as $\epsilon \to 0$).

In the following, we motivate our mathematical setting by heuristically explaining why a vortex is a natural pattern in thin-films with circular cross-section. The pattern formation is driven by the balance between the exchange energy and the full stray-field energy penalizing both volume and surface charges (see Section 1.3 for a more detailed view on the connection to physics). The micromagnetic principle of "pole avoidance" states that there are no volume charges or surface charges at the mesoscopic level, i.e., the limit magnetization m_0 satisfies

$$|m_0| = 1, \ \ \nabla \cdot m_0 = 0 \quad \text{in} \quad B^2 \quad \text{and} \quad m_0 \cdot \nu = 0 \quad \text{on} \quad \partial B^2. \tag{6}$$

Now an important remark concerns the rigidity of problem (6) for having smooth solutions. Indeed, in terms of the stream function $m_0 = \nabla^\perp \psi_0$, (6) turns into a Dirichlet problem for the eikonal equation:

$$|\nabla \psi_0| = 1 \quad \text{in} \quad B^2 \quad \text{and} \quad \psi_0 = 0 \quad \text{on} \quad \partial B^2. \tag{7}$$

The method of characteristics then implies the nonexistence of smooth solutions of (7). Obviously, there are infinitely many continuous solutions that satisfy (7) in the sense of distributions. A crucial issue is that the "viscosity solution" of (7) given by $\psi_0(x) = \mathrm{dist}(x, \partial B^2)$ corresponds to the vortex configuration

$$m_0 = \frac{x^\perp}{|x|} \qquad \text{in } B^2,$$

the so called "Landau state" in micromagnetic terminology. One particularity of the vortex m_0 is that it admits $BV-$liftings φ (i.e. $m_0 = e^{i\varphi}$ in B^2) and every $BV-$lifting of minimal total variation has a jump set concentrated on a radius of the unit disc (see [5], [12]). This jump set J is an idealization of a 360° Néel wall at the mesoscopic level. Indeed, at the microscopic level, J is replaced by a 360° Néel wall where the magnetization turns counter clockwise around the orthogonal direction at J and the quick transition takes place on a small scale ϵ. Therefore, understanding the structure and energy cost of these types of 360° Néel walls is important for our aim.

360° Néel walls. A Néel wall is a sharp one-dimensional transition layer connecting two mesoscopic directions of the magnetization. It is characterized by the angle between these two directions (called *wall angle*) and the rotation is performed in-plane. Néel walls exhibit a two-scale structure: Most of the rotation of the magnetization takes place in a small core, enclosed by two logarithmically decreasing tails with slow variation of the magnetization [21, 22]. Without confining the tails of the Néel wall, they will spread out, thus leading to vanishing energy in the limit [7]. Hence, typically, the tails of the Néel wall are confined either by material anisotropy, by finiteness of the sample or by neighboring Néel walls. The Néel walls we consider in the following are confined by the boundary of the sample.

For the aim of the paper, we will address the special case of 360° Néel walls. In these walls, the magnetization performs a complete rotation across the transition layer. They are characterized by the angle $\alpha \in [0, 2\pi)$ between the mesoscopic direction of the magnetization and the normal direction to the wall (see Figure 2). We call these transition layers "360° Néel walls of initial angle α". Note that for any Néel wall with a wall angle smaller than 360°, the condition to be charge free

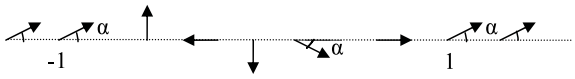

Figure 2: 360° Néel wall of initial angle α.

uniquely determines the initial angle α. For 360° Néel walls, the situation is different: In this case, charge free transition layers can be achieved for any initial angle α. Our analysis shows that the initial angle α contributes to the leading order energy of the 360° Néel wall. Another peculiarity of 360° Néel walls (of initial angle $\alpha > 0$) with respect to general Néel walls resides in their internal structure. The 360° Néel wall consists of two parts with zero magnetic net charge. This means that these two parts only interact by weak dipole–dipole interaction. For this reason the thickness of the 360° Néel wall is much larger than the thickness of the 180° Néel wall. A detailed numerical analysis of the 360° Néel wall, also including the effect of anisotropy and external field, can be found in [24].

We fix the setting to describe one–dimensional transition layers. We will assume that the magnetization $m = (u, v) : \mathbb{R} \to S^1$ only depends on a single variable $t \in \mathbb{R}$. In this case, the specific

one-dimensional energy associated to m in our model reduces to the following expression:

$$E_\epsilon^{1d}(m) = \epsilon \int_{\mathbb{R}} \frac{1}{1-u^2} |\frac{d}{dt}u|^2 \, dt + \frac{|\ln \epsilon|}{2} \int_{\mathbb{R}} ||\frac{d}{dt}|^{1/2}u|^2 \, dt. \tag{8}$$

For our analysis of 360° Néel walls, we assume that the initial direction of the magnetization is given by the angle $\alpha \in [0, 2\pi)$ and a complete rotation is imposed by the following condition:

$$m(t) = e^{i\alpha} \quad \text{for } |t| \geq 1 \quad \text{and} \quad \deg(m) = 1.$$

In other words, using the lifting $m = e^{i\varphi}$, the above condition is equivalent to

$$\varphi(t) = \alpha \quad \text{for } t \leq -1, \qquad \varphi(t) = 2\pi + \alpha \quad \text{for } t \geq 1. \tag{9}$$

We finally remark that 360° Néel walls are a commonly observed structure in thin magnetic films, see [11, p. 457]. They typically arise from (global) topological constraints: These can be related to the geometry of the magnetic sample. Our analysis indicates that the 360° Néel wall is a global minimizing structure for our sample geometry. Note however that commonly 360° Néel walls occur as metastable states [11].

1.2 Main results

Our first result concerns the exact leading order energy of a 360° Néel wall with initial angle α.

Theorem 1.1. *Let $m_\epsilon : \mathbb{R} \to S^1$ be a minimizer of (8) satisfying (9). Then m_ϵ is a smooth map inside $(-1, 1)$ and its energetic cost is given by*

$$E_\epsilon^{1d}(m_\epsilon) = \pi \, (1 + \cos^2 \alpha) + o(1) \qquad \text{as } \epsilon \to 0. \tag{10}$$

The result shows that even within the class of 360° Néel walls there is a dependence of the energy in terms of the leading order constant with respect to the initial angle α. This result agrees well with a numerical simulation in [24, Fig. 2]. In particular, the energetic difference between the two extreme cases $\alpha = 0$ and $\alpha = \pi/2$ by a factor 2 is predicted by the graph in [24, Fig. 2]. Note that we have smoothness in the interior for any critical point to the energy functional (8).

The main result in this paper, characterizes asymptotically, the energy of the vortex:

Theorem 1.2. *Let $\{m_\epsilon\}$ be a minimizing family in (5). Then we have*

$$E_\epsilon^{2d}(m_\epsilon) = 2\pi + o(1) \qquad \text{as } \epsilon \to 0.$$

In this sense, we have $E_0^{2d}(x^\perp/|x|) = 2\pi$.

Note that this result includes the precise leading constant of the minimal energy. Our construction for the upper bound of the energy is based on the inclusion of a single 360° Néel wall of initial angle 0 along a radius of the disk.

On the other hand, we prove the lower bound of a vortex in a slightly more general context. More precisely, as in [17], we consider localized stray fields $h : B^3 \to \mathbb{R}^3$ determined by static Maxwell's equation in the weak sense: For all $\zeta \in C_c^\infty(B^3)$,

$$\int_{B^3} h \cdot (\nabla, \frac{\partial}{\partial z})\zeta \, dxdz = \int_{B^2} \nabla \cdot m \, \zeta \, dx, \tag{11}$$

where $B^3 \subset \mathbb{R}^3$ is the unit ball in $\mathbb{R}^3$ and the localized micromagnetic energy

$$E_\epsilon^{loc}(m, h) = \epsilon \int_{B^2} |\nabla m|^2 \, dx + |\ln \epsilon| \int_{B^3} |h|^2 \, dxdz.$$

Obviously, $E_\epsilon^{loc}(m, h_{ac}) \leq E_\epsilon^{2d}(m)$. We will prove the following estimate for the localized energy:

Theorem 1.3. *Let $\{m_\epsilon\}$ be a family satisfying (5) and let $h_\epsilon : B^3 \to \mathbb{R}^3$ be localized stray fields associated to m_ϵ by (11). Then we have*

$$E^{loc}_\epsilon(m_\epsilon, h_\epsilon) \;\geq\; 2\pi + o(1) \qquad\qquad \text{as } \epsilon \to 0.$$

1.3 Physical relevance

In this section we explain the validity of our reduced model together with the relevance of the vortex structure (driven by a $360°-$Néel wall) as a global minimizer in a regime of ultra-thin films. For a soft magnetic body $\Omega \subset \mathbb{R}^3$, in the absence of anisotropy and external magnetic field, the Landau–Lifshitz micromagnetic energy is given by:

$$E^{3d}(m) = d^2 \int_\Omega |(\nabla, \frac{\partial}{\partial z})m|^2 \; dxdz + \int_{\mathbb{R}^3} |(\nabla, \frac{\partial}{\partial z})U(m)|^2 \; dxdz. \tag{12}$$

In this model, the magnetization $m = (m', m_3) : \mathbb{R}^3 \to \mathbb{R}^3$ satisfies $|m| = 1$ in Ω and $m = 0$ outside of Ω. The material parameter d is called exchange length and is of order of nanometers. The full stray-field potential $U(m) : \mathbb{R}^3 \to \mathbb{R}$ is defined by Maxwell's equations,

$$\int_{\mathbb{R}^3} (\nabla, \frac{\partial}{\partial z})U(m) \cdot (\nabla, \frac{\partial}{\partial z})\zeta \; dxdz = \int_{\mathbb{R}^3} (\nabla, \frac{\partial}{\partial z}) \cdot m \; \zeta \; dxdz, \quad \text{for every } \zeta \in C^\infty_c(\mathbb{R}^3). \tag{13}$$

We are interested in ferromagnetic samples in the shape of a thin circular film, i.e. $\Omega = B_\ell \times (0, t)$ where $B_\ell \subset \mathbb{R}^2$ is the disc of radius ℓ. The model includes three length scales: the film thickness t, the diameter of film ℓ and the exchange length d. This leads to the following two dimensionless parameters:

$$\epsilon := \frac{d^2}{\ell t} \qquad\qquad \text{and} \qquad\qquad \eta := \frac{t}{\ell}.$$

(ϵ can be interpreted as the size of the core of a Néel wall, while η is the aspect ratio of the micromagnetic sample.) We claim that our model is a good approximation of the full energy (12) in the following regime of ultra thin-films:

$$\epsilon, \eta \ll 1 \quad \text{and} \quad \ln|\ln\eta| \ll \frac{1}{\epsilon|\ln\epsilon|} \ll |\ln\eta|. \tag{14}$$

It means that η is exponentially small with respect to ϵ; in particular, $\eta \ll \epsilon$ which leads to $t \ll d \ll \ell$.

In the following we will explain this assertion with both rigorous and heuristic arguments, see also [18, 8]: The main issue is the asymptotic behavior of the energy in the regime of ultra– thin films. We first nondimensionalize in length with respect to ℓ, i.e. $(\bar{x}, \bar{z}) = (\frac{x}{\ell}, \frac{z}{\ell})$, $\bar{m}(\bar{x}, \bar{z}) = m(x, z)$, $\bar{U}(\bar{m})(\bar{x}, \bar{z}) = \frac{1}{\ell} U(m)(x, z)$ and $\bar{E}^{3d}(\bar{m}) = \frac{1}{\ell^3} E^{3d}(m)$. Skipping the $^-$, we get

$$E^{3d}(m) = \epsilon\eta \int_{B^2\times(0,\eta)} |(\nabla, \frac{\partial}{\partial z})m|^2 \; dxdz + \int_{\mathbb{R}^3} |(\nabla, \frac{\partial}{\partial z})U(m)|^2 \; dxdz. \tag{15}$$

We make two assumptions which are enforced by the penalization of exchange energy for minimizers with energy bounded as in Theorem 1.2. We assume that:

(a) m varies on length scales $\gg \eta$.

(b) $m = m(x)$, i.e. m is $z-$invariant.

With these assumptions, (15) can be approximated by the following reduced energy (see [4, 8, 18]):

$$\begin{aligned} E^{red}(m) = \epsilon\eta^2 \int_{B^2} |\nabla m|^2 \, dx + \frac{\eta^2}{2} \|(\nabla \cdot m')_{ac}\|^2_{\dot{H}^{-1/2}(\mathbb{R}^2)} \\ + \frac{1}{2\pi}\eta^2 |\ln \eta| \int_{\partial B^2} (m' \cdot \nu)^2 \, d\mathcal{H}^1 + \eta \int_{B^2} m_3^2. \end{aligned} \tag{16}$$

The above formula follows by explicitly solving the stray field equation in Fourier variables; this is possible due to assumption b), for thickness independent m (see [18], [13]). In Fourier variables (and in view of assumption a)), it then can be seen that the stray-field energy asymptotically decomposes into three terms in the thin-film regime: one is penalizing the volume charges $(\nabla \cdot m')_{ac}$ as an homogeneous $\dot{H}^{-1/2}-$norm (equal with the stray-field energy created by $h_{ac}(m)$, explained in Introduction), a second term penalizing the lateral charges $m' \cdot \nu$ in the L^2-norm, as well as the third term that counts the surface charges m_3 on the top and bottom of the cylinder.

In order to ensure $m' \cdot \nu = 0$ at ∂B^2 in the limit $\epsilon \to 0$ and $\eta \to 0$, there are three different structures that typically appear in our regime (14): Néel walls, Bloch lines and boundary vortices. We explain these structures in the following and compare their respective energies. The comparison of these energies motivates the regime (14). There also exists a fourth structure, the asymmetric Bloch wall, but we do not discuss it here since the asymmetric Bloch wall is more expensive than a Néel wall in the considered regime $t \ll d$.

As already mentioned in Section 1.1, the structure of a Néel wall consists of two regions: a core ($|x_1| \lesssim w_{core} = O(\epsilon)$) and two logarithmic decaying tails ($w_{core} \lesssim |x_1| \lesssim w_{tail} = O(1)$). The energetic cost (by unit length) of a Néel wall is given by

$$E^{red}(\text{Néel wall}) = O(\frac{\eta^2}{|\ln \epsilon|})$$

with the exact prefactor $\pi(1 - \cos(\theta/2))^2/2$ where θ is the wall angle (see Lemma 3.5 or [14]).

A Bloch line is a regularization of a vortex on the microscopic level of the magnetization that is fully out-of-plane at the center. The prototype of a Bloch line is given by a vector field

$$m : B^2 \to S^2$$

defined in a circular cross-section B^2 of a thin-film and satisfying:

$$\nabla \cdot m' = 0 \text{ in } B^2 \qquad \text{and} \qquad m'(x) = x^\perp \text{ on } \partial B^2. \tag{17}$$

Here, the Bloch line is assumed to be invariant in the vertical direction and the word "line" refers

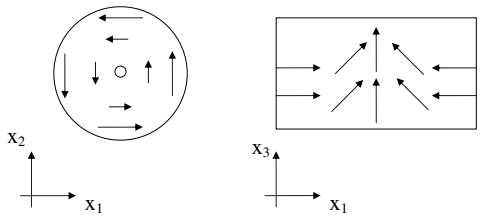

Figure 3: Bloch line.

to that direction. Since the magnetization turns in-plane at the boundary of the disk B^2, a localized

region is created, the core of the Bloch line, where the magnetization becomes perpendicular to the horizontal plane (see Figure 3). The reduced energy (16) for a magnetization (17) writes as:

$$E^{red}(m) = \epsilon\eta^2 \int_{B^2} |\nabla m|^2 \, dx + \eta \int_{B^2} m_3^2 \, dx.$$

The Bloch line corresponds to the minimizer of this energy under the constraint (17). Observe that the competition between the exchange and the stray field energy (by the penalization of surface charges) implies that the size of the core of the Bloch line is of order $\sqrt{\epsilon\eta}$. Since $|\nabla m'| \leq |\nabla m|$ and $1 \geq m_3^2 \geq m_3^4 = (1-|m'|^2)^2$, the reduced energy has a lower bound given by the Ginzburg-Landau type functional:

$$\epsilon\eta^2 GL_{\sqrt{\epsilon\eta}}(m') \leq E^{red}(m),$$

where

$$GL_\lambda(m') = \int_{B^2} |\nabla m'|^2 \, dx + \frac{1}{\lambda^2} \int_{B^2} (1-|m'|^2)^2 \, dx, \tag{18}$$

with $\lambda > 0$ a small parameter. The minimization of (18) is performed over all magnetizations $m' \in H^1(B^2, \mathbb{R}^2)$ such that $m'(x) = x^\perp$ on ∂B^2. In view of the theory developed in [2], the minimal energy of (18) is $2\pi|\ln\lambda| + O(1)$. Since the structure of the minimizer of GL_λ is divergence-free in B^2 for small λ (see [25]), we deduce that the cost of a Bloch line is given by

$$E^{red}(\text{Bloch line}) = O(\epsilon\eta^2|\ln(\epsilon\eta)|)$$

with the exact prefactor π.

Next we address boundary vortices. A boundary vortex corresponds to an in-plane transition of the magnetization along the boundary from $\nu^\perp$ to $-\nu^\perp$, see Figure 4. The corresponding minimization problem is given by

$$E^{red}(m) = \epsilon\eta^2 \int_{B^2} |\nabla m|^2 \, dx + \frac{1}{2\pi}\eta^2|\ln\eta| \int_{\partial B^2} (m' \cdot \nu)^2 \, d\mathcal{H}^1$$

within the set of in–plane magnetizations $m \in H^1(B^2, S^1)$ (i.e., $m_3 = 0$). The minimizer of this energy is an harmonic map with values in S^1 driven by a pair of boundary vortices. These have been analyzed in [20, 23]. The transition is regularized on the length scale of the exchange part of the energy, i.e. the core of the boundary vortex has length of $O(\frac{\epsilon}{|\ln\eta|})$. The cost of such a transition is given by

$$E^{red}(\text{Boundary vortex}) = O(\epsilon\eta^2|\ln(\epsilon/|\ln\eta|)|)$$

with exact prefactor π.

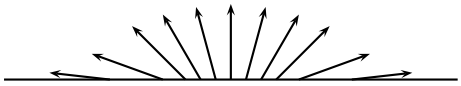

Figure 4: A boundary vortex

Our regime (14) is equivalent to the following ordering of energies:

$$E^{red}(\text{Boundary vortex}) \ll E^{red}(\text{Néel wall}) \ll E^{red}(\text{Bloch line}).$$

Therefore, when minimizing E^{red}, Bloch lines are avoided, since they are too expensive. Instead, our regime corresponds to the energy level of Néel walls; The boundary vortices do not contribute to the energy in highest order. In particular, our vortex structure is driven by a 360° Néel wall accompanied by a pair of boundary vortices at ∂B^2.

In view of energy (16), a more physical model to consider is the following: In the regime (14), minimize over the set of configurations $m : B^2 \to S^1$ the functional energy

$$\epsilon\eta^2 \int_{B^2} |\nabla m|^2 \, dx + \frac{\eta^2}{2} \|(\nabla \cdot m')_{ac}\|^2_{\dot{H}^{-1/2}(\mathbb{R}^2)} + \frac{1}{2\pi}\eta^2 |\ln \eta| \int_{\partial B^2} (m' \cdot \nu)^2 \, d\mathcal{H}^1. \tag{19}$$

We conjecture that the vortex is the minimizer of the above variational problem. While we cannot rigorously prove that, we would like to compare the vortex with another typical structure observed in thin ferromagnetic discs, the so called S–state (see [11]). We show that the vortex has asymp-

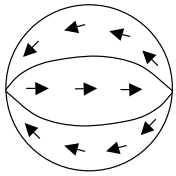

Figure 5: S-state.

totically lower energy than the S–state, thus indicating that the vortex might be indeed global minimizer of the energy. Recall that the vortex corresponds to the viscosity solution of the domain B^2, i.e.

$$m_0(x) = \nabla^\perp \operatorname{dist}(x, \partial B^2).$$

In our regime, renormalizing energy E^{red} by $\eta^2/|\ln \epsilon|$ (so that Néel walls have order one energy per unit length), the asymptotic cost of a vortex follows by Theorem 1.2:

$$E_0(m_0) = 2\pi.$$

The limit configuration for $\epsilon = 0$ of the S–state is represented by

$$S(x) = \begin{cases} \nabla^\perp \operatorname{dist}(x, \partial B^2_+) & \text{if } x \in B^2_+ \\ -\nabla^\perp \operatorname{dist}(x, \partial B^2_-) & \text{if } x \in B^2_-, \end{cases}$$

where $B^2_\pm = \{x \in B^2 : \pm x_2 \geq 0\}$ are the upper (resp. lower) half–discs. In order to compute the asymptotic energetic cost of S, we denote by θ, the wall angle between two mesoscopic directions m^+ and m^- in S^1, i.e. $m^+ = e^{i\theta} m^-$. Furthermore, we denote the corresponding asymptotic energy density of a Néel wall connecting the directions m^+ and m^- by $e(m^+, m^-) = \frac{\pi}{2}(1 - \cos\frac{\theta}{2})^2$. Then

$$E_0(S) = \int_\gamma e(S^+, S^-) \, d\mathcal{H}^1$$

where γ denotes the jump set of the $S-$state, i.e.

$$\gamma = \gamma^+ \cup \gamma^- \quad \text{and} \quad \gamma^\pm(x_1) = (x_1, \pm\frac{1 - x_1^2}{2}) \text{ with } x_1 \in (-1, 1).$$

In fact, if we denote by $S^{\pm}$ the traces of S on γ, one has $S^{-}(x) = (1,0)$ and $S^{+}(x) = \pm\frac{x^{\perp}}{|x|}$ for $x \in \gamma^{\pm}$ and therefore, by the change of variable $x_1 = \tan\frac{t}{2}$ we get

$$\begin{aligned}\int_{\gamma} e(S^+,S^-)\,d\mathcal{H}^1 = 2\int_{\gamma^+} e(S^+,S^-)\,d\mathcal{H}^1 &= \pi\int_{-1}^{1}(1-\frac{x_1}{\sqrt{1+x_1^2}})^2\sqrt{1+x_1^2}\,dx_1\\ &= \pi\int_0^{\pi/2}\frac{1+\sin^2\frac{t}{2}}{\cos^3\frac{t}{2}}\,dt = 2\pi[\frac{\sin\frac{t}{2}}{\cos^2\frac{t}{2}}]_0^{\pi/2} = 2\sqrt{2}\pi.\end{aligned}$$

The above computation concludes the proof showing that the S–state is less favorable than the vortex state in the regime (14). It is an open question to rigorously prove that the vortex state indeed is the global minimizer over all planar configurations of (19).

1.4 Related analysis

A related functional arising in the context of micromagnetics has been introduced and analyzed by Rivière and Serfaty in [26, 27]. In these papers, the authors consider the following energy

$$RS_\epsilon(m) \;=\; \epsilon\int_\Omega |\nabla m|^2\,dx + \frac{1}{\epsilon}\int_{\mathbb{R}^2} ||\nabla|^{-1}\nabla\cdot(m\mathbb{1}_\Omega)|^2\,dx, \tag{20}$$

for unit–valued configurations $m \in H^1(\Omega, S^1)$ defined in a planar domain $\Omega \subset \mathbb{R}^2$. Physically, (20) describes the energy of a ferromagnetic sample with shape of an infinitely extended cylinder, i.e. $\Omega\times\mathbb{R}$. By assuming m is independent of the vertical z–direction, the micromagnetic energy (12) indeed reduces to a fully two–dimensional problem, given by (20). In [26, 27], the authors show Γ–converge to a limiting energy RS_0. This energy is concentrated on lines, furthermore it measures discontinuities of the phase φ of m rather than of the magnetization m. They also show that for disc shaped sample, the vortex configuration $\pm m_0$ is asymptotically the global minimizer and they calculate its energy. Our aim is to shown that for our model, the limit energy E_0 for the vortex has the same features: it is concentrated on a jump line and it is a function of the phase rather than the magnetization.

However, there is an important difference in the qualitative character of the line-energy. For a small jump of size $\theta \ll 1$ of the phase φ along a line-discontinity, the limit energy density scales cubically, i.e. $RS_0 \sim \theta^3$ (see [26, p. 9]). However, in our case, a line-energy of φ is connected to the corresponding jump energy density of the 360° Néel wall. It hence has a quartic scale, i.e. $E_0 \sim \theta^4$, cf. Theorem 1.1 (see also [14]). For this reason, we cannnot rely on entropy methods as in [26], since the entropy production typically scales cubically for small jumps [8]. We mention that a theory of Lipschitz entropies has also been developed for Bloch walls (see [15]) in order to derive their quadratic energetic cost in the jump size.

In the following, we would like to comment on the relationship of our analysis to the well–known analysis on Ginzburg–Landau vortices (see [2]). As described in the previous section, in the case of thicker ferromagnetic films, the minimizer is expected to have a Bloch line structure rather than the 360° Néel wall. In this case, the corresponding minimization problem is a variant of the Ginzburg–Landau problem (18). The constraint $|(m_1,m_2)| = 1$ is relaxed for the planar components of m by penalizing the distance of (m_1,m_2) to S^1. There is a big qualitative difference for the microscopic structure of a vortex: in the case of the Ginzburg–Landau model, it has a core of size ϵ in the center where the in-plane magnetization vanishes, while in our case it stays with values in S^1 and concentrates on a radius at the same scale ϵ (a line discontinuity of the lifting connecting the center of the vortex with the boundary). This is related to the fact that the main contribution of the energy in the case of the Ginzburg–Landau energy is represented by the exchange energy away from the vortex core, while in our case the main contribution of the energy derives from the

nonlocal stray field part of the energy (as indicated by the construction for the Néel wall). For this reason, it is not possible to use the techniques developed for the Ginzburg–Landau theory.

We finally note that there has been further research on Modica–Mortola type problems where the homogeneous H^{-1}–norm in (20) is replaced by the homogeneous $H^{1/2}$–norm. One of these models addresses the dislocations in crystals [19, 10]. Furthermore, in the context of phase separation the classical Cahn–Hilliard energy has been extended by an $H^{1/2}$–term, for references see [1].

2 Preliminaries

In this section, we give basic interpolation inequalities upon which our proofs of the lower bounds for the energy are based.

First, we recall standard definitions and properties for some homogeneous Sobolev spaces, see [28]. Let $s \in \mathbb{R}$ and $u : \mathbb{R}^N \to \mathbb{R}$ be a tempered distribution in $\mathcal{S}'(\mathbb{R}^N)$. We denote the homogeneous $\dot{H}^s$-seminorm of u by

$$\|u\|_{\dot{H}^s}^2 := \int_{\mathbb{R}^N} |\xi|^{2s} |\mathcal{F}(u)|^2(\xi)\, d\xi,$$

where $\mathcal{F}(u) \in \mathcal{S}'(\mathbb{R}^N)$ stands for the Fourier transform of u (as a tempered distribution), i.e.

$$\mathcal{F}(u)(\xi) \;=\; \frac{1}{(2\pi)^{N/2}} \int_{\mathbb{R}^N} e^{-i\xi\cdot x} u(x)\, dx, \qquad\qquad \forall \xi \in \mathbb{R}^N.$$

These quantities can be also characterized as trace seminorms. In particular,

$$\|u\|_{\dot{H}^{1/2}(\mathbb{R}^N)}^2 \;:=\; \frac{1}{2} \inf_{\substack{U \in \dot{H}^1(\mathbb{R}^{N+1}) \\ U_{|\mathbb{R}^N \times \{0\}} = u}} \|U\|_{\dot{H}^1(\mathbb{R}^{N+1})}^2. \tag{21}$$

Another equivalent representation of the fractional Sobolev seminorm $s = 1/2$ is given by difference quotients:

$$\|u\|_{\dot{H}^{1/2}(\mathbb{R})}^2 \;=\; \frac{1}{2\pi} \int_{\mathbb{R}} \int_{\mathbb{R}} \frac{|u(x) - u(y)|^2}{|x-y|^2}\, dxdy. \tag{22}$$

Note that the last two characterizations naturally generalize to smooth bounded domains and also to the case of periodic functions (in particular when the domain is the unit circle S^1).

Our proofs for the lower bounds of vortex and Néel wall energy are based on the following duality argument and a variant of an interpolation inequality which holds (asymptotically) with exact leading order constant. The idea is to estimate the dual product $(\chi, \sigma)_{L^2(\mathbb{R}^N)}$ for a trial function χ (controlling the length of orbits generated by $m^\perp$ if $N = 2$) and a function σ (standing for the volume charges $(\nabla \cdot m)\mathbb{1}_{B^2}$ in our physical context). In the limit $\epsilon/w \to 0$, one has

$$\begin{aligned} \big|(\chi, \sigma)_{L^2(\mathbb{R}^N)}\big|^2 \;\le\; & \frac{2 + o(1)}{\pi}\, \ln \frac{w}{\epsilon}\, \|\chi\|_{L^\infty(\mathbb{R}^N)} \|\nabla \chi\|_{\mathcal{M}(\mathbb{R}^N)} \\ & \times \big(\epsilon \|\sigma\|_{L^2(\mathbb{R}^N)}^2 + \|\sigma\|_{\dot{H}^{-1/2}(\mathbb{R}^N)}^2 + \frac{1}{w} \|\sigma\|_{\dot{H}^{-1}(\mathbb{R}^N)}^2\big), \end{aligned} \tag{23}$$

where the Landau symbol $o(1)$ represents a function that converges to zero as $\epsilon/w \to 0$ uniformly in all other unknowns (in particular the speed of convergence does not depend on σ and χ). The above quantity is best understood as a variation of a duality estimate in the spaces $\dot{H}^{1/2}(\mathbb{R}^N)$ and $\dot{H}^{-1/2}(\mathbb{R}^N)$. In fact, the energy (1) yields a slightly higher control on σ (depending of ϵ) than its

$\dot{H}^{-1/2}(\mathbb{R}^N)-$seminorm, whereas $(\|\chi_\epsilon\|_{L^\infty}\|\nabla\chi_\epsilon\|_{\mathcal{M}})$ has the same scaling as $\|\chi_\epsilon\|^2_{\dot{H}^{1/2}}$ but is slightly weaker. In fact, the rate of the failing interpolation embedding

$$BV\cap L^\infty(\mathbb{R}^N)\not\subset \dot{H}^{1/2}(\mathbb{R}^N)$$

is logarithmic: Regularizing the $\dot{H}^{1/2}(\mathbb{R}^N)-$seminorm, this perturbation gives a weaker seminorm that is controlled with a logarithmically slow rate having the optimal prefactor $\frac{2}{\pi}$ (see [6]): For $\epsilon\ll w$,

$$\int_{\mathbb{R}^N}\min\{\frac{1}{\epsilon},|\xi|,w|\xi|^2\}|\mathcal{F}(\chi)|^2\,d\xi\lessapprox\frac{2}{\pi}\left(\ln\frac{w}{\epsilon}\right)\|\chi\|_{L^\infty}\,\|\nabla\chi\|_{\mathcal{M}(\mathbb{R}^N)}.$$

The parameters ϵ (resp. w) correspond to a cut–off for high (resp. low) frequencies.

A variant of (23) for dimension $N=2$ is given in [6, p. 249]. The proof extends directly to (23). For dimension $N=1$, (23) can be written conveniently in terms of the 1–d energy (8) (see e.g. [14]):

Lemma 2.1. *Let $m:\mathbb{R}\to\mathbb{R}^2$ with $|m|\le 1$ in $\mathbb{R}$ and let $\chi:\mathbb{R}\to\mathbb{R}$ be a function of locally bounded variation. Let $\sigma=\frac{dm_1}{dx_1}\mathbb{1}_{(-1,1)}$ (standing for the divergence of m). Then we have*

$$\left|(\chi,\sigma)_{L^2(\mathbb{R})}\right|\ \le\ \left((\frac{4}{\pi}+o(1))\|\chi\|_{L^\infty(\mathbb{R})}\|\nabla\chi\|_{\mathcal{M}(\mathbb{R})}\ (E^{1d}_\epsilon(m)+o(1))\right)^{1/2}\qquad as\quad \epsilon\to 0. \tag{24}$$

The above inequality does not include w in contrary to (23). The reason is that w corresponds to a low frequency cut–off which is not needed in the case of uniformly bounded support of $\nabla\cdot m$. More precisely, (24) corresponds to (23) when we set $w:=|\ln\epsilon|^2$ and $N=1$ since

$$\lim_{\epsilon\to 0}\frac{|\ln\epsilon|}{|\ln\epsilon/w|}\ =\ 1\qquad\qquad\text{and}\qquad\qquad\frac{1}{w}\|\sigma\|^2_{\dot{H}^{-1}(\mathbb{R})}\ \le\ \frac{\|m_1\|^2_{L^2(-1,1)}}{|\ln\epsilon|^2}\ =\ o(1).$$

Note that the change of the prefactor from $2/\pi$ in (23) to $4/\pi$ in (24) is consequence of the factor $1/2$ in (3) coming for the stray field energy in (8).

The localized version of (23) for $N=2$ was proved in [17]. We state it in a particular case:

Lemma 2.2. *Let $m:B^2\to\mathbb{R}^2$, $\sigma=\nabla\cdot m$ and $\chi:\mathbb{R}^2\to\{\pm1\}$ be a function of locally bounded variation. We consider $\eta\in C^\infty_c(B^3)$ with $0\le\eta\le 1$ and let $h:B^3\to\mathbb{R}^3$ be a stray field associated to m by (11). Then there exists a universal constant $C>0$ such that for all $\epsilon\in(0,1]$,*

$$\begin{aligned}\left|\int_{B^2}\eta^2\ \chi\ \nabla\cdot m\ dx\right|\ \le\ &\left(\frac{4|\ln\epsilon|}{\pi}\|\chi\|_{L^\infty(B^2)}\|\eta^2\nabla\chi\|_{\mathcal{M}(B^2)}\ \int_{B^3}\eta^2|h|^2\right)^{1/2}\\ &+\frac{C(1+\|\nabla\eta\|_{C^0})(1+\|\eta\nabla\chi\|_{\mathcal{M}(B^2)})}{|\ln\epsilon|^{1/2}}E^{loc}_\epsilon(m,h)^{1/2}.\end{aligned} \tag{25}$$

The idea of the localization is that in the limit $\epsilon\to 0$ only the jump part of $\nabla\chi$, but not of the derivative of the cut-off function η is seen in highest order (i.e. in line (25)). This holds true as long as the derivative of η stays bounded.

3 360° Neel wall

This section is concerned with 1–d 360° transition layers with prescribed initial angle α. In Section 3.1, we first show smoothness of critical points of the energy (8). We then give matching upper and lower bound for the energy in Sections 3.2 and 3.3. In this section, we always assume that m only depends on one variable $t:=x_1$ and satisfies (9). We write $m(t)=(u(t),v(t))$.

3.1 Smoothness

We first show how (8) follows from the 2–d energy (1): The calculation for the exchange part of the energy is trivial and follows directly from $|m| = 1$. We hence only show the derivation for the stray field part of the energy: Since the magnetization only depends on $t = x_1$, in view of (2) it is clear that the stray-field h associated to m only depends on t and z and furthermore the third component of h is zero. Identifying h with a 2–d vector field, i.e. $h = (h_1, h_3)$, (2) takes the following form

$$\begin{cases} (\frac{\partial}{\partial t}, \frac{\partial}{\partial z}) \times h = 0 & \text{for} \quad (t,z) \in \mathbb{R}^2, \\ (\frac{\partial}{\partial t}, \frac{\partial}{\partial z}) \cdot h = 0 & \text{in} \quad \{z \neq 0\}, \\ [h_3] = -\frac{du}{dt} & \text{on} \quad \{z = 0\}, \end{cases} \tag{26}$$

where $[\cdot]$ denotes the jump size over the horizontal line $\{z = 0\}$. The unique solution $h \in L^2(\mathbb{R}^2, \mathbb{R}^2)$ of (26) can be explicitly computed in terms of its Fourier transform with respect to t (see e.g. [9]):

$$\mathcal{F}(h(\cdot, z))(\xi) = e^{-|\xi||z|} \mathcal{F}(\frac{du}{dt})(\xi) \left(\frac{i\xi}{2|\xi|}, -\frac{\text{sign}(z)}{2} \right), \quad \xi \neq 0, z \neq 0.$$

A straightforward computation then shows that

$$\int_{\mathbb{R}^2} |h|^2 \, dtdz = \frac{1}{2} \int_{\mathbb{R}} ||\frac{d}{dt}|^{1/2} u|^2 \, dt.$$

thus concluding the derivation of (8). It is convenient to express (8) in terms of the lifting φ, i.e. $(u, v) = (\cos\varphi, \sin\varphi)$. We get

$$E_\epsilon^{1d}(m) = \epsilon \int_{\mathbb{R}} |\, \frac{d}{dt}\varphi|^2 \, dt + \frac{|\ln\epsilon|}{2} \int_{\mathbb{R}} ||\, \frac{d}{dt}|^{1/2} \cos\varphi|^2 \, dt. \tag{27}$$

It follows that the Euler–Lagrange equation in weak formulation is given by:

$$\int_{\mathbb{R}} \left(\epsilon \, \frac{d}{dt}\varphi \;\; \frac{d}{dt}\zeta - |\ln\epsilon| b(t) \sin\varphi \;\, \zeta \right) \, dt \;\; = \;\; 0, \qquad \text{for all } \zeta \in C_c^\infty(-1,1), \tag{28}$$

where we have defined the non–local operator $b(t)$ by

$$b(t) \;\; := \frac{1}{2} \; (-\Delta)^{1/2} (\cos\varphi - \cos\alpha), \qquad \text{i.e.} \qquad \mathcal{F}(b)(\xi) = |\xi| \mathcal{F}(\cos\varphi - \cos\alpha). \tag{29}$$

Note that since we have imposed Dirichlet boundary conditions (9), the identity (28) is only valid in the interior of the domain $(-1, 1)$. Let us also remark that $b(t)$ can be interpreted as the trace of the first component h_1 of the stray field on the horizontal line $\{z = 0\}$.

The existence of a minimizer of (27) with Dirichlet boundary conditions of type (9) is standard since (27) is lower semicontinuous with respect to the weak-topology in $H^1_{loc}(\mathbb{R})$. The smoothness of the 180°−Néel wall (on the entire real axis) was shown in [21, Lemma 1] in the case where the Néel wall is confined by anisotropy (see also [3]). The proof in our model (where the Néel wall is confined by the interaction with the sample edges) is based on the arguments used in [3]. However, in contrary to [3], we need to use a localization argumentent since the solution is not smooth at the boundary. In the following, we show the smoothness of every critical point of the energy (27):

Lemma 3.1 (Smoothness)**.** *Let $\epsilon > 0$ and $\alpha \in [0, 2\pi)$. Every weak solution $\varphi \in \dot{H}^1(\mathbb{R})$ of (28) satisfying the boundary conditions (9) is smooth in $(-1, 1)$, i.e. $\varphi \in C^\infty((-1, 1))$ and is a classical solution of*

$$\epsilon \;\; \frac{d^2}{dt^2}\varphi + |\ln\epsilon| b(t) \sin\varphi \;\; = \;\; 0, \qquad \text{for } t \in (-1, 1). \tag{30}$$

Proof. Since $\varphi \in \dot{H}^1(\mathbb{R})$ is a weak solution of (28), this already means that (30) is satisfied in the distributional sense. It remains to show that $\varphi \in C^\infty((-1,1))$.

Since $\varphi \in \dot{H}^1(\mathbb{R})$, we have $\cos\varphi \in \dot{H}^1(\mathbb{R})$. In particular $\varphi \in H^1((-1,1))$ and by (29) we also have $b \in L^2(\mathbb{R})$. We want to show that for any fixed $R \in (0,1)$ and any fixed $k \in \mathbb{N}$, we have

$$\varphi \in H^{k+1}((-R,R)), \qquad \text{and} \qquad b \in H^k((-R,R)). \tag{31}$$

By standard Sobolev embedding theorems, smoothness of φ and b in $(-1,1)$ then follow from (31). In order to show (31), we argue by induction. Fixing $\delta = (1-R)/(2k+2) > 0$, we may assume that we have

$$\varphi \in H^k((-R-2\delta, R+2\delta)), \qquad \text{and} \qquad b \in H^{k-1}((-R-2\delta, R+2\delta)). \tag{32}$$

In view of (30), (32) immediately yields $\varphi \in H^{k+1}((-R-2\delta, R+2\delta))$. It remains to show that $b \in H^k((-R,R))$. For this, we apply a localization argument on the (nonlocal) equation (29):

Choose a smooth cut–off function ζ with $\zeta = 1$ in $(-R-\delta, R+\delta)$ and $\zeta = 0$ outside $(-R-2\delta, R+2\delta)$. We localize the right hand side of (29), i.e. let $f := (\cos\varphi - \cos\alpha)$ and decompose $f = f_0 + f_1$, where $f_0 := f\zeta$. Since (29) is linear, we have $b = b_0 + b_1$ where $b_j := (-\Delta)^{1/2} f_j$, $j = 1,2$. Since $f_0 \in H^{k+1}(\mathbb{R})$, it immediately follows by (29) that $b_0 \in H^k(\mathbb{R})$. Therefore in order to get (31), we need to show that $b_1 \in H^k((-R,R))$.

We first note that by (32), we have $b_1 \in H^{k-1}((-R-2\delta, R+2\delta))$. Using a duality argument, we will show $b_1 \in H^k((-R,R))$, i.e. we claim that

$$(b_1, \frac{d^k}{dt^k}\eta)_{L^2} \;\le\; C(R)\, \|\eta\|_{L^2}, \qquad \text{for every } \eta \in C_c^\infty(-R,R).$$

Indeed, in using the definition of b_1 and the explicit expression (22) of the $H^{1/2}$ scalar product, we get

$$\begin{aligned}
(b_1, \frac{d^k}{dt^k}\eta)_{L^2} &= \frac{1}{2\pi}\int_{\mathbb{R}}\int_{\mathbb{R}} \frac{(f_1(t)-f_1(s))(\frac{d^k}{dt^k}\eta(t) - \frac{d^k}{ds^k}\eta(s))}{(t-s)^2}\, dt\, ds \\
&= \frac{-1}{\pi}\int_{\operatorname{supp} f_1}\int_{\operatorname{supp}\eta} \frac{f_1(t)\,\frac{d^k}{ds^k}\eta(s)}{(t-s)^2}\, dt\, ds \\
&= C_k \int_{\operatorname{supp} f_1}\int_{\operatorname{supp}\eta} \frac{f_1(t)\eta(s)}{(t-s)^{k+2}}\, dt\, ds \\
&\le \frac{C_k}{\delta^{k+2}} \|f_1\|_{L^2(\mathbb{R})}\|\eta\|_{L^2}.
\end{aligned}$$

In the above estimate, we have used that the two sets $\operatorname{supp} f_1 \subset [-1, -R-\delta) \cup (R+\delta, 1]$ and $\operatorname{supp}\eta \subset (-R,R)$ have distance $\ge \delta$. This concludes the proof of (31) and hence of the lemma. □

3.2 Upper bound

In this section, we prove the upper bound in Theorem 1.1. For this, we construct a recovery family for the 360°−Néel wall of initial angle α. The main result is:

Proposition 3.2. *Let $\alpha \in [0, 2\pi)$. Then there exists $m_\epsilon : \mathbb{R} \to S^1$ satisfying (9) and*

$$E_\epsilon^{1d}(m_\epsilon) \;\le\; \pi\,(1+\cos^2\alpha) + o(1) \qquad \text{as } \epsilon \to 0.$$

The construction of the 360°−Néel wall with initial angle α is based on the following idea: The full rotation 360° rotation splits up into two rotations of size 2α and $2\pi - 2\alpha$, respectively. Each of these rotations is (up to minor modifications) represented a rescaled 180°–Néel wall profile, see Figure 6 (see [7]).

For $\delta > 0$, we introduce the "bump" function w_δ by

$$w_\delta(t) = \begin{cases} \frac{1}{|\ln \delta|} \ln \frac{1}{\sqrt{t^2+\delta^2}} & \text{if } |t| \le \sqrt{1-\delta^2}, \\ 0 & \text{if } |t| \ge \sqrt{1-\delta^2}, \end{cases} \tag{33}$$

see also the left hand side of Figure 6. Here and in the following, we use the parameter δ as a short notation for

$$\delta = \epsilon |\ln \epsilon|.$$

a)

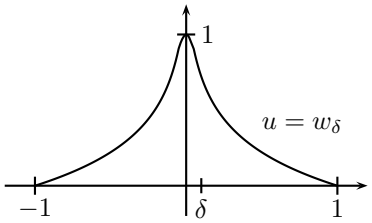

b)

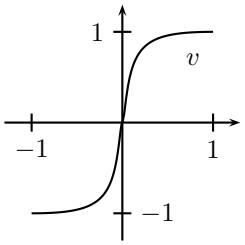

Figure 6: Profiles of the 180° Néel wall with magnetization $m = (u, v)$

Based on w_δ, we define for each $\beta \in [0, 2]$, the following S^1–valued magnetization $(u_\beta, v_\beta) : \mathbb{R} \to S^1$ by

$$u_\beta(t) = \begin{cases} (1-\beta) + \beta w_\delta(t) & \text{if } |t| \le \sqrt{\frac{1}{4} - \delta^2}, \\ \cos \theta_{\delta,\beta}(|t|) & \text{if } \sqrt{\frac{1}{4} - \delta^2} \le |t| \le 1, \\ 1 - \beta & \text{if } |t| \ge 1, \end{cases} \text{ and } v_\beta(t) = \begin{cases} -\sqrt{1 - u_\beta^2(t)} & \text{if } t < 0, \\ \sqrt{1 - u_\beta^2(t)} & \text{if } t > 0. \end{cases} \tag{34}$$

Here, $\theta_{\delta,\beta} : [\sqrt{1/4 - \delta^2}, 1] \to \mathbb{R}$ is the linear function satisfying

$$\theta_{\delta,\beta}\big(\sqrt{1/4 - \delta^2}\big) \;=\; \arccos(1 - \beta + \beta \frac{\ln 2}{|\ln \delta|}) \quad \text{and} \quad \theta_{\delta,\beta}(1) = \arccos(1 - \beta).$$

Our 360° Néel wall construction is based on two such rescaled functions $(u_{\beta_j}, v_{\beta_j})$. Before giving the proof of Proposition (3.2), we first give the corresponding energy estimates for the profile (u_β, v_β):

Lemma 3.3. *For $\beta \in [0, 2]$, we have that*

$$\int_{\mathbb{R}} |\, \frac{d}{dt}(u_\beta, v_\beta)|^2 \; dt = o(\frac{1}{\epsilon |\ln \epsilon|}) \quad \textit{and} \quad \int_{\mathbb{R}} || \, \frac{d}{dt}|^{1/2} u_\beta|^2 \; dt \le \frac{\beta^2 \pi + o(1)}{|\ln \epsilon|} \quad \textit{as} \;\; \epsilon \to 0.$$

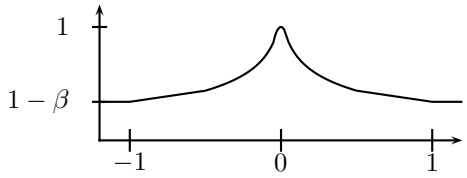

Figure 7: Sketch of u_β

Proof. We divide the proof in several steps:

Step 1. We first estimate the exchange energy of the profile:

$$\begin{aligned}\int_{\mathbb{R}} |\frac{d}{dt}(u_\beta, v_\beta)|^2\, dt &= \int_{\{\sqrt{\frac{1}{4}-\delta^2}\le|t|\le 1\}} |\frac{d}{dt}\theta_{\delta,\beta}|^2 + \beta^2 \int_{\{|t|\le\sqrt{\frac{1}{4}-\delta^2}\}} \frac{1}{1-u_\beta^2}|\frac{d}{dt}w_\delta|^2 \\ &= I + II.\end{aligned}$$

We distinguish two cases:

Case 1. $\beta \in [0,2)$. For estimating I, if $\beta = 0$ then $\theta_{\delta,\beta}$ is constant, hence

$$I = \int_{\{|t|\ge\sqrt{\frac{1}{4}-\delta^2}\}} |\frac{d}{dt}\theta_{\delta,\beta}|^2 = 0.$$

Otherwise, $\beta \in (0,2)$ and we estimate for $t \in (\sqrt{\frac{1}{4}-\delta^2}, 1)$,

$$\begin{aligned}|\frac{d}{dt}\theta_{\delta,\beta}| &= \frac{|\arccos(1-\beta+\beta\frac{\ln 2}{|\ln\delta|}) - \arccos(1-\beta)|}{1-\sqrt{\frac{1}{4}-\delta^2}} \\ &\lesssim |\arccos(1-\beta+\beta\frac{\ln 2}{|\ln\delta|}) - \arccos(1-\beta)| \\ &\lesssim \frac{1}{\sqrt{1-(1-\beta)^2}}\frac{\beta\ln 2}{|\ln\delta|} \lesssim \frac{1}{|\ln\delta|}, \end{aligned} \tag{35}$$

where $\epsilon > 0$ (and $\delta > 0$) is small enough. Hence,

$$I = \int_{\{1\ge|t|\ge\sqrt{\frac{1}{4}-\delta^2}\}} |\frac{d}{dt}\theta_{\delta,\beta}|^2 \lesssim \frac{1}{|\ln\delta|^2} = o(\frac{1}{\epsilon|\ln\epsilon|}) \quad \text{as} \quad \epsilon\to 0.$$

For the estimate of II, we have $1+u_\beta \ge 2-\beta > 0$ if $\beta \in [0,2)$. Therefore,

$$1-u_\beta^2 \gtrsim 1-u_\beta = \frac{\beta\ln\frac{t^2+\delta^2}{\delta^2}}{2|\ln\delta|}$$

By a change of variable ($t = \delta s$), this yields

$$\begin{aligned}II = \beta^2 \int_{\{|t|\le\sqrt{\frac{1}{4}-\delta^2}\}} \frac{1}{1-u_\beta^2}|\frac{d}{dt}w_\delta|^2 &\lesssim \frac{1}{|\ln\delta|}\int_0^1 \frac{t^2}{(t^2+\delta^2)^2\ln\frac{t^2+\delta^2}{\delta^2}}\, dt \\ &\lesssim \frac{1}{\delta|\ln\delta|}\int_0^\infty \frac{s^2}{(s^2+1)^2\ln(s^2+1)}\, ds \\ &\lesssim \frac{1}{\epsilon|\ln\epsilon|^2} = o(\frac{1}{\epsilon|\ln\epsilon|}) \quad \text{as} \quad \epsilon\to 0.\end{aligned}$$

(Here, we used that $s \mapsto \frac{s^2}{(s^2+1)^2\ln(s^2+1)} \in L^1(\mathbb{R}_+)$.) That proves the desired exchange energy estimate in the case $\beta \in [0,2)$.

Case 2. $\beta = 2$. For estimating I, we use that for $t \in (\sqrt{\frac{1}{4}-\delta^2}, 1)$,

$$|\frac{d}{dt}\theta_{\delta,\beta}| = \frac{|\arccos(-1+2\frac{\ln 2}{|\ln\delta|}) - \arccos(-1)|}{1-\sqrt{\frac{1}{4}-\delta^2}} \lesssim |\arccos(-1+2\frac{\ln 2}{|\ln\delta|}) - \pi| \lesssim \sqrt{\frac{1}{|\ln\delta|}}, \quad (36)$$

where $\epsilon > 0$ is small enough. (Here, we used the inequality $|\arccos(-1+t)-\pi| \le 2\sqrt{t}$ for $t \in [0,1]$.) Hence,

$$I = \beta^2 \int_{\{|t| \ge \sqrt{\frac{1}{4}-\delta^2}\}} |\frac{d}{dt}\theta_{\delta,\beta}|^2 \lesssim \frac{1}{|\ln\delta|} = o(\frac{1}{\epsilon|\ln\epsilon|}) \quad \text{as} \quad \epsilon \to 0.$$

For the estimate of II, we have $1-u_\beta^2 = 4w_\delta(1-w_\delta)$ and therefore, the change of variable $t = \delta s$ yields

$$\begin{aligned} II = \beta^2 \int_{\{|t| \le \sqrt{\frac{1}{4}-\delta^2}\}} \frac{1}{1-u_\beta^2}|\frac{d}{dt}w_\delta|^2 &\lesssim \int_0^{1/2} \frac{t^2}{(t^2+\delta^2)^2 \ln\frac{1}{t^2+\delta^2}\ln\frac{t^2+\delta^2}{\delta^2}}\, dt \\ &\lesssim \frac{1}{\delta}\int_0^{\frac{1}{2\delta}} \frac{s^2}{(s^2+1)^2(\ln\frac{1}{\delta^2} - \ln(s^2+1))\ln(s^2+1)}\, ds \\ &= II_1 + II_2 + II_3, \end{aligned}$$

where II_1, II_2 and II_3 represent the splitting of the last integral into the three intervals $(0,1)$, $(1, |\ln\delta|)$ and $(|\ln\delta|, \frac{1}{2\delta})$, respectively. We compute:

$$II_1 \lesssim \frac{1}{\delta}\int_0^1 \frac{1}{\ln\frac{1}{\delta^2} - \ln 2}\, ds \lesssim \frac{1}{\delta|\ln\delta|} = o(\frac{1}{\epsilon|\ln\epsilon|}),$$

$$II_2 \lesssim \frac{1}{\delta|\ln\delta|}\int_1^{|\ln\delta|} \frac{ds}{s^2} \lesssim o(\frac{1}{\epsilon|\ln\epsilon|})$$

(since $\ln\frac{1}{\delta^2} - \ln(s^2+1) \gtrsim \ln\frac{1}{\delta}$ for $1 < s < |\ln\delta|$) and

$$II_3 \lesssim \frac{1}{\delta}\int_{|\ln\delta|}^{\frac{1}{2\delta}} \frac{ds}{s^2} = o(\frac{1}{\epsilon|\ln\epsilon|}) \quad \text{as} \quad \epsilon \to 0$$

(since $\ln\frac{1}{\delta^2} - \ln(s^2+1) \gtrsim 1$ for $\frac{1}{2\delta} > s > |\ln\delta|$). Summing up, we deduce the first estimate in Lemma 3.3 for $\beta = 2$.

Step 2. We now estimate the stray-field energy of the profile (u_β, v_β). For that, we extend u_β into $\mathbb{R}^2$ by the following radially symmetric function $U_\beta : \mathbb{R}^2 \to \mathbb{R}$ defined as $U_\beta(x_1,x_2) = u_\beta(\sqrt{x_1^2+x_2^2})$ for every $(x_1,x_2) \in \mathbb{R}^2$. Using the estimate of the $\dot{H}^{1/2}-$seminorm of u_β as a trace of U_β, we deduce:

$$\begin{aligned} \int_{\mathbb{R}} ||\frac{d}{dt}|^{1/2} u_\beta|^2\, dt \le \frac{1}{2}\int_{\mathbb{R}^2} |\nabla U_\beta|^2\, dx &= \pi\int_0^1 |\frac{du_\beta}{dr}|^2\, rdr \\ &= \pi\int_0^{\sqrt{\frac{1}{4}-\delta^2}} |\frac{du_\beta}{dr}|^2\, rdr + \pi\int_{\sqrt{\frac{1}{4}-\delta^2}}^1 \sin^2\theta_{\delta,\beta}\, |\frac{d\theta_{\delta,\beta}}{dr}|^2\, rdr. \end{aligned}$$

The change of variable $r = \delta s$ leads to the following bound for the first term of the above RHS:

$$\int_0^{\sqrt{\frac{1}{4}-\delta^2}} |\frac{du_\beta}{dr}|^2 \, rdr \leq \frac{\beta^2}{|\ln\delta|^2}\int_0^1 \frac{r^3\,dr}{(r^2+\delta^2)^2} \leq \frac{\beta^2}{|\ln\delta|^2}\int_0^{1/\delta}\frac{s^3\,ds}{(s^2+1)^2} = \frac{\beta^2+o(1)}{|\ln\delta|}.$$

For the second term on $(\sqrt{\frac{1}{4}-\delta^2}, 1)$ of the RHS, we distinguish two cases:

Case 1. $\beta \in [0,2)$. If $\beta = 0$, then $\frac{d\theta_{\delta,\beta}}{dr} = 0$ on $(\sqrt{\frac{1}{4}-\delta^2}, 1)$, therefore the estimate is trivial. If $\beta \in (0,2)$, then we use (35) and it implies that

$$\int_{\sqrt{\frac{1}{4}-\delta^2}}^1 \sin^2\theta_{\delta,\beta}\,|\frac{d\theta_{\delta,\beta}}{dr}|^2\,rdr \lesssim \frac{1}{|\ln\delta|^2}.$$

Case 2. $\beta = 2$. We have that

$$\sin^2\theta_{\delta,\beta}(t) \leq \sin^2\theta_{\delta,\beta}(\sqrt{\frac{1}{4}-\delta^2}) = 1-(1-\frac{2\ln 2}{|\ln\delta|})^2 = O(\frac{1}{|\ln\delta|}) \quad \text{for} \quad t \in (\sqrt{\frac{1}{4}-\delta^2}, 1).$$

Combining with (36), it follows as before that

$$\int_{\sqrt{\frac{1}{4}-\delta^2}}^1 \sin^2\theta_{\delta,\beta}\,|\frac{d\theta_{\delta,\beta}}{dr}|^2\,rdr \lesssim \frac{1}{|\ln\delta|^2}.$$

Therefore, we conclude that

$$\int_{\mathbb{R}} ||\frac{d}{dt}|^{1/2}u_\beta|^2\,dt \leq \frac{\pi\beta^2+o(1)}{|\ln\delta|} = \frac{\pi\beta^2+o(1)}{|\ln\epsilon|} \quad \text{as} \quad \epsilon\to 0.$$

□

We now prove the main result of this section:

Proof of Proposition 3.2 . We combine two transition profiles

$$(u_1,v_1) := (u_{\beta_1}, v_{\beta_1}) \qquad \text{and} \qquad (u_2,v_2) := (u_{\beta_2}, v_{\beta_2})$$

defined as in (34) where β_j, $j = 1,2$, is given by

$$\beta_1 := 1+\cos\alpha \qquad \text{and} \qquad \beta_2 := 1-\cos\alpha.$$

The first transition profile represents a rotation of $(2\pi - 2\alpha)$ while the second one represents a rotation of 2α. Our construction for $m = (u,v)$ is sketched in Figure. 8. It is defined as follows: If $\alpha \in [0,\pi)$, we define

$$u(t) = \begin{cases} -u_1(4(t+\frac{1}{2})) & \text{if } t<0,\\ u_2(4(t-\frac{1}{2})) & \text{if } t>0,\end{cases} \quad \text{and} \quad v(t) = \begin{cases} -v_1(4(t+\frac{1}{2})) & \text{if } t<0,\\ v_2(4(t-\frac{1}{2})) & \text{if } t>0.\end{cases}$$

Otherwise if $\alpha \in [\pi, 2\pi)$, we set

$$u(t) = \begin{cases} u_2(4(t+\frac{1}{2})) & \text{if } t<0,\\ -u_1(4(t-\frac{1}{2})) & \text{if } t>0,\end{cases} \quad \text{and} \quad v(t) = \begin{cases} v_2(4(t+\frac{1}{2})) & \text{if } t<0,\\ -v_1(4(t-\frac{1}{2})) & \text{if } t>0.\end{cases}$$

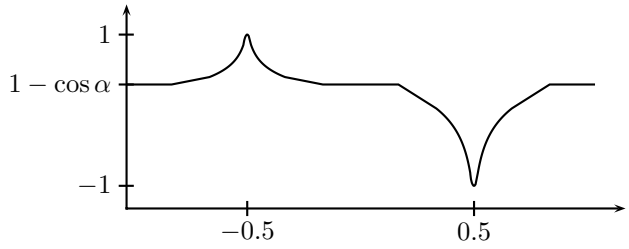

Figure 8: Sketch of u for 360° Néel wall construction

For the exchange energy of m, Lemma 3.3 yields by rescaling:

$$\epsilon \int_{\mathbb{R}} |\frac{d}{dt} m|^2 \, dt \;=\; 4\epsilon \sum_{j=1,2} \int_{\mathbb{R}} |\frac{d}{dt}(u_j, v_j)|^2 \, dt \;=\; o(\frac{1}{|\ln \epsilon|}).$$

For the stray-field energy, it is sufficient to show that

$$\int_{\mathbb{R}} |\,|\frac{d}{dt}|^{1/2} u|^2 \, dt \;\le\; \sum_{j=1,2} \int_{\mathbb{R}} |\,|\frac{d}{dt}|^{1/2} u_j|^2 \, dt + o(\frac{1}{|\ln \epsilon|}), \tag{37}$$

since Lemma 3.3 will then yield

$$\frac{1}{2} \int_{\mathbb{R}} |\,|\frac{d}{dt}|^{1/2} u|^2 \, dt \;\le\; \frac{\pi(\beta_1^2 + \beta_2^2) + o(1)}{2|\ln \epsilon|} \;=\; \frac{\pi(1 + \cos^2 \alpha) + o(1)}{|\ln \epsilon|} \quad \text{as} \;\; \epsilon \to 0.$$

In order to show (37), we denote by $f(t) = u(t) - \cos\alpha$, $f_1(t) = -u_1(4(t + \frac{1}{2})) - \cos\alpha$ and $f_2(t) = u_2(4(t + \frac{1}{2})) - \cos\alpha$ for every $t \in \mathbb{R}$. Then we notice that

$$f \;=\; f_1 + f_2 \quad \text{in } \mathbb{R}, \quad \mathcal{H}^1(\operatorname{supp} f_1) = \mathcal{H}^1(\operatorname{supp} f_2) \;\le\; \frac{1}{2} \quad \text{and} \quad \operatorname{dist}(\operatorname{supp} f_1, \operatorname{supp} f_2) \;\ge\; \frac{1}{2}.$$

Moreover,

$$\int_{\mathbb{R}} |\,|\frac{d}{dt}|^{1/2} u|^2 \, dt \;=\; \int_{\mathbb{R}} |\,|\frac{d}{dt}|^{1/2} f|^2 \, dt \quad \text{and} \quad \int_{\mathbb{R}} |\,|\frac{d}{dt}|^{1/2} u_j|^2 \, dt \;=\; \int_{\mathbb{R}} |\,|\frac{d}{dt}|^{1/2} f_j|^2 \, dt,$$

for $j = 1, 2$. We compute that

$$\begin{aligned} \int_{\mathbb{R}} |\,|\frac{d}{dt}|^{1/2} f|^2 \, dt \;&=\; \frac{1}{2\pi} \int_{\mathbb{R}} \int_{\mathbb{R}} \frac{|f(s) - f(t)|^2}{|s - t|^2} \, ds dt \\ &=\; \sum_{j=1,2} \int_{\mathbb{R}} |\,|\frac{d}{dt}|^{1/2} f_j|^2 \, dt + \frac{1}{\pi} \int_{\operatorname{supp} f_1} \int_{\operatorname{supp} f_2} \frac{-f_1(s) f_2(t)}{|s - t|^2} \, ds dt. \end{aligned}$$

Since f_1 and f_2 have opposite sign and their supports have distance $\ge 1/2$ between each other, (37) follows by the estimate:

$$\begin{aligned} \int_{\operatorname{supp} f_1} \int_{\operatorname{supp} f_2} \frac{-f_1(s) f_2(t)}{|s - t|^2} \, ds dt \;&\lesssim\; \sum_{j=1,2} \int_{\operatorname{supp} f_j} |f_j(t)|^2 \, dt \\ &\lesssim\; \int_{\mathbb{R}} |w_\delta(t)|^2 \, dt + O(\frac{1}{|\ln \delta|^2}) = o(\frac{1}{|\ln \epsilon|}). \end{aligned}$$

□

3.3 Lower bound

In this section we give the proof for the lower bound in Theorem 1.1. The main idea for the proof is the following: Consider any admissible configuration $m_\epsilon = (u_\epsilon, v_\epsilon)$ satisfying (9) for some given initial angle α. We first give an optimal lower bound separately for the regions where u_ϵ is positive respectively nonnegative. We then use the fact that the "interaction" of the nonlocal magnetostatic component of the energy is positive between these two regions.

Since

$$E_\epsilon^{1d}(m_\epsilon) \;\geq\; \tilde{E}_\epsilon^{1d}(u_\epsilon) \;:=\; \epsilon \int_{\mathbb{R}} |\, \frac{d}{dt} u_\epsilon|^2 \; dt + \frac{|\ln \epsilon|}{2} \int_{\mathbb{R}} ||\, \frac{d}{dt}|^{1/2} u_\epsilon|^2 \; dt, \tag{38}$$

it is enough to prove the lower bound for $\tilde{E}_\epsilon^{1d}$ rather than E_ϵ^{1d}:

Proposition 3.4. *Let $\alpha \in [0, 2\pi)$ and $m_\epsilon = (u_\epsilon, v_\epsilon) : \mathbb{R} \to S^1$ satisfy (9). Then*

$$\tilde{E}_\epsilon^{1d}(u_\epsilon) \;\geq\; \pi \; (1 + \cos^2 \alpha) + o(1) \qquad \text{as } \epsilon \to 0.$$

Proof. Let

$$\tilde{u}_\epsilon \;:=\; u_\epsilon - \cos\alpha.$$

Although the energy $\tilde{E}_\epsilon^{1d}$ is non–local, it behaves super-additively with respect to its positive and negative components. Indeed, let

$$f_\epsilon := (\tilde{u}_\epsilon)_+ = \max\{\tilde{u}_\epsilon, 0\} \quad \text{and} \quad g_\epsilon := (\tilde{u}_\epsilon)_- = \min\{\tilde{u}_\epsilon, 0\}$$

be the positive and negative part, respectively of $\tilde{u}_\epsilon$. In particular.

$$\tilde{u}_\epsilon \;=\; f_\epsilon + g_\epsilon. \tag{39}$$

We claim that

$$\tilde{E}_\epsilon^{1d}(\tilde{u}_\epsilon) \;\geq\; \tilde{E}_\epsilon^{1d}(f_\epsilon) + \tilde{E}_\epsilon^{1d}(g_\epsilon). \tag{40}$$

Indeed, the first term in (38) is additive with respect to (39) since the support of f_ϵ and g_ϵ is of zero-measure:

$$\int_{\mathbb{R}} |\, \frac{d}{dt} \tilde{u}_\epsilon|^2 \; dt = \int_{\mathbb{R}} |\, \frac{d}{dt} f_\epsilon|^2 \; dt + \int_{\mathbb{R}} |\, \frac{d}{dt} g_\epsilon|^2 \; dt.$$

For the second term in (38), the super-additivity is a consequence of the following representation of the stray field energy:

$$\begin{aligned}
\int_{\mathbb{R}} ||\, \frac{d}{dt}|^{1/2} \tilde{u}_\epsilon|^2 \; dt &\overset{(22)}{=} \frac{1}{2\pi} \int_{\mathbb{R}} \int_{\mathbb{R}} \frac{|\tilde{u}_\epsilon(t) - \tilde{u}_\epsilon(s)|^2}{|t-s|^2} \; dt \; ds \\
&= \int_{\mathbb{R}} ||\, \frac{d}{dt}|^{1/2} f_\epsilon|^2 \; dt + \int_{\mathbb{R}} ||\, \frac{d}{dt}|^{1/2} g_\epsilon|^2 \; dt + \frac{1}{\pi} \int_{\operatorname{supp} f_\epsilon} \int_{\operatorname{supp} g_\epsilon} \frac{-f_\epsilon(t) g_\epsilon(s)}{|t-s|^2} \; dt ds \\
&\geq \int_{\mathbb{R}} ||\, \frac{d}{dt}|^{1/2} f_\epsilon|^2 \; dt + \int_{\mathbb{R}} ||\, \frac{d}{dt}|^{1/2} g_\epsilon|^2 \; dt,
\end{aligned}$$

where in the last line of the above estimate we have used that $f_\epsilon g_\epsilon \leq 0$. The above computations show that (40) holds. Since $\sup \tilde{u}_\epsilon = \sup |f_\epsilon| = 1 - \cos\alpha$ and $\inf \tilde{u}_\epsilon = -\sup |g_\epsilon| = -1 - \cos\alpha$, Lemma 3.5 below, applied for f_ϵ and g_ϵ shows that

$$\begin{aligned}
\tilde{E}_\epsilon^{1d}(f_\epsilon) \;&\geq\; \frac{\pi}{2} \; (1 - \cos\alpha)^2 + o(1) \quad \text{as } \epsilon \to 0, \\
\tilde{E}_\epsilon^{1d}(g_\epsilon) \;&\geq\; \frac{\pi}{2} \; (1 + \cos\alpha)^2 + o(1) \quad \text{as } \epsilon \to 0.
\end{aligned} \tag{41}$$

Combining (40) and (41), we conclude that

$$\tilde{E}_\epsilon^{1d}(\tilde{u}_\epsilon) \overset{(40)}{\geq} \frac{\pi}{2}\left((1-\cos\alpha)^2+(1+\cos\alpha)^2\right)+o(1) \overset{(41)}{=} \pi\,(1+\cos^2\alpha)+o(1).$$

□

The next result gives the optimal control on the height of a transition by the energy:

Lemma 3.5. *Let $\beta \geq 0$. Suppose that $\tilde{u}_\epsilon : \mathbb{R} \to \mathbb{R}$ be a continuous function that satisfies $\sup|\tilde{u}_\epsilon| = \beta$ and $\tilde{u}_\epsilon = 0$ for $|x| \geq 1$. Then*

$$\tilde{E}_\epsilon^{1d}(\tilde{u}_\epsilon) \geq \frac{\beta^2\pi}{2}+o(1) \qquad \text{as } \epsilon \to 0.$$

Proof. This lemma is a rescaled version of a corresponding 2–d result in [6]. Let t_0 be a point where $\tilde{u}_\epsilon(t_0) = \beta$. We define the test function $\chi \in BV_{loc}(\mathbb{R})$ by

$$\chi(t) = +1 \text{ for } t \leq t_0 \qquad\qquad \chi(t) = -1 \text{ for } t > t_0.$$

Using integration by parts, Lemma 2.1 yields

$$\begin{aligned} 2\beta &= \left|\int_{\mathbb{R}} \chi\ \frac{d}{dt}\tilde{u}_\epsilon\ dt\right| \leq \left(\frac{4}{\pi}\ \|\chi\|_{L^\infty(\mathbb{R})}\|\nabla\chi\|_{\mathcal{M}(\mathbb{R})}\ (\tilde{E}_\epsilon^{1d}(\tilde{u}_\epsilon)+o(1))\right)^{1/2} \\ &\leq \left(\frac{8}{\pi}\ (\tilde{E}_\epsilon^{1d}(\tilde{u}_\epsilon)+o(1))\right)^{1/2}, \end{aligned}$$

thus concluding the proof. □

4 Vortex

We start by constructing a recovery family in order to deduce the upper bound for the energy of a vortex.

4.1 Upper bound

Proposition 4.1. *There exists a family $\{m_\epsilon \in H^1(B^2,S^1)\}_{\epsilon>0}$ satisfying (4) and such that the following upper bound holds true:*

$$E_\epsilon^{2d}(m_\epsilon) \ \leq\ 2\pi+o(1) \qquad \text{as } \epsilon \to 0.$$

Proof. In dependence of $0 < \epsilon \ll 1$, we will use the two small parameters

$$\lambda = \lambda(\epsilon) = \frac{1}{|\ln\epsilon|^2} \qquad \text{and} \qquad \delta = \delta(\epsilon) = \epsilon|\ln\epsilon|^3. \tag{42}$$

In order to construct the profile m_ϵ, we distinguish three regions, see Figure 9.:

$$D_1 = B^2 \setminus (D_2 \cup D_3),$$
$$D_2 = \{x \in B^2\ :\ \lambda < |x| < 1, x_2 \geq 0, |x_1| \leq \lambda\} \quad \text{and} \quad D_3 = \{x \in B^2\ :\ |x| < \lambda\}.$$

In the region D_1, m_ϵ will coincide with the vortex (in particular m_ϵ is divergence free). In the region D_2, the profile will turn clockwise as a 360°−Néel wall of initial angle 0, and the region D_3

Figure 9: Decomposition of B_1 and sketch of minimizer

stands for the core of the vortex, where we apply some linear cut–off in the radius for the phase of m_ϵ.

Step 1. Construction. Throughout the proof, we denote the phase of m_ϵ by Φ_ϵ, i.e. $m_\epsilon = e^{i\Phi_\epsilon}$. In D_1, the profile m_ϵ is defined as follows:

$$m_\epsilon(x) = e^{i\Phi_\epsilon(x)} = \frac{x^\perp}{|x|} \qquad \text{in } D_1,$$

or equivalently, in polar coordinates, the phase is given by $\Phi_\epsilon(r,\theta) = \theta$ in D_1. In D_2, we first denote by $(\tilde{u}_\delta, \tilde{v}_\delta) = e^{i\tilde{\varphi}_\delta} : \mathbb{R} \to S^1$, the following approximation of the 360°−Néel wall of initial angle 0 (magnetization turning in clockwise direction

$$\tilde{u}_\delta(t) = \begin{cases} 1 - 2w_\delta(t) & \text{if } |t| \le \sqrt{\frac{1}{4} - \delta^2} \\ \cos\tilde{\theta}_\delta(|t|) & \text{if } \sqrt{\frac{1}{4} - \delta^2} \le |t| \le 1 \\ 1 & \text{if } |t| \ge 1, \end{cases} \quad \text{and} \quad \tilde{v}_\delta(t) = \begin{cases} -\sqrt{1 - \tilde{u}_\delta^2(t)} & \text{if } t < 0, \\ \sqrt{1 - \tilde{u}_\delta^2(t)} & \text{if } t > 0, \end{cases} \tag{43}$$

where w_δ is defined in (33) and $\tilde{\theta}_\delta : [\sqrt{1/4 - \delta^2}, 1] \to [0, \frac{\pi}{2}]$ is defined by

$$\tilde{\theta}_\delta \;:=\; \text{linear function with} \quad \tilde{\theta}_\delta\big(\sqrt{1/4 - \delta^2}\big) \;=\; \arccos\frac{|\ln 4\delta|}{|\ln \delta|} \quad \text{and} \quad \tilde{\theta}_\delta(1) = 0. \tag{44}$$

In view of (43), we may assume that $\tilde{\varphi}_\delta(0) = -\pi$. We then have $\tilde{\varphi}_\delta(-\infty) = 0$ and $\tilde{\varphi}_\delta(+\infty) = -2\pi$ and since $\tilde{\varphi}_\delta + \pi$ is antisymmetric in t, we also get

$$\tilde{\varphi}_\delta(-t) + \tilde{\varphi}_\delta(t) = -2\pi \qquad \text{for every } \; t \in \mathbb{R}. \tag{45}$$

We rescale the transition layer $(\tilde{u}_\delta, \tilde{v}_\delta)$ in order to be contained in D_2: For each arc with $r \in (\lambda, 1)$ fixed in D_2 and where the angle varies in the interval $\theta \in (\frac{\pi}{2} \pm \arcsin\frac{\lambda}{r})$, we define the rescaled transition layer (u_ϵ, v_ϵ) with phase φ_ϵ by

$$(u_\epsilon, v_\epsilon)(\theta) \;=\; e^{i\varphi_\epsilon(\theta)} \;:=\; (\tilde{u}_\delta, \tilde{v}_\delta)\left(\frac{\theta - \frac{\pi}{2}}{\arcsin\lambda}\right),$$

or equivalently, the rescaled phase is given by

$$\varphi_\epsilon(\theta) = \tilde{\varphi}_\delta\left(\frac{\theta - \frac{\pi}{2}}{\arcsin\lambda}\right). \tag{46}$$

The profile m_ϵ is defined in terms of its components in radial direction $\vec{r}$ and angular direction $\vec{\theta}$ for rotation around arcs with fixed radius,

$$m_\epsilon(r,\theta) \;=\; e^{i\Phi_\epsilon(r,\theta)} \;=\; u_\epsilon(\theta)\vec{\theta} - v_\epsilon(\theta)\vec{r} \qquad\qquad \text{in } D_2.$$

Notice that in D_2 (as well as in D_1), the profile m_ϵ (together with its phase Φ_ϵ) are invariant in r. Also, we have the following relation between φ_ϵ and Φ_ϵ:

$$\Phi_\epsilon(r,\theta) \;=\; \theta + \varphi_\epsilon(\theta) + \frac{\pi}{2} \qquad\qquad \text{in } D_2. \tag{47}$$

Our construction is such that the phase Φ_ϵ is continuous in $D_1 \cup D_2$ since $\Phi_\epsilon(r,0) = \Phi_\epsilon(r,2\pi) = \frac{\pi}{2}$ for $r \in [\lambda, 1)$. Finally, in the core region D_3, we define the profile $m_\epsilon(r,\theta) = e^{i\Phi_\epsilon(r,\theta)}$ in polar coordinates by

$$\Phi_\epsilon(r,\theta) \;=\; \frac{r}{\lambda}\Phi_\epsilon(\lambda,\theta) \qquad\qquad \text{in } D_3, \tag{48}$$

where we recall by (47) that $\Phi_\epsilon(\lambda,\theta) = \theta + \frac{\pi}{2} + \tilde{\varphi}_\delta(\frac{\theta-\frac{\pi}{2}}{\arcsin\lambda})$ for every $\theta \in (0, 2\pi)$.

Step 2. Exchange energy estimate. We first estimate the exchange energy of m_ϵ. In D_1, we have $|\nabla m_\epsilon| = 1/r$ in polar coordinates and hence

$$\epsilon \int_{D_1} |\nabla m_\epsilon|^2 \, dx \;\le\; 2\pi\epsilon \int_\lambda^1 \frac{dr}{r} \;=\; O(\epsilon|\ln\lambda|) \;=\; o(\frac{1}{|\ln\epsilon|}).$$

In D_2, we compute

$$|\nabla m_\epsilon|^2 \;=\; |\nabla\Phi_\epsilon|^2 \overset{(47)}{\lesssim} \frac{1}{r^2}\left(1 + \big(\frac{d}{d\theta}\varphi_\epsilon\big)^2(\theta)\right) \;=\; \frac{1}{r^2}\left(1 + \frac{(\frac{d}{d\theta}\tilde{\varphi}_\delta)^2(\frac{\theta-\frac{\pi}{2}}{\arcsin\lambda})}{\arcsin^2\lambda}\right), \tag{49}$$

which implies by Lemma 3.3 that

$$\begin{aligned}
\epsilon \int_{D_2} |\nabla m_\epsilon|^2 \, dx &\overset{(49)}{\lesssim} \epsilon \int_\lambda^1 \int_{\frac{\pi}{2}-\arcsin\frac{\lambda}{r}}^{\frac{\pi}{2}+\arcsin\frac{\lambda}{r}} (1 + (\frac{d}{d\theta}\varphi_\epsilon)^2(\theta)) \, d\theta \frac{dr}{r} \\
&\overset{(46)}{\lesssim} \epsilon \int_\lambda^1 \left(\arcsin\frac{\lambda}{r}\right)\frac{dr}{r} + \frac{\epsilon}{\arcsin\lambda}\left(\int_\lambda^1 \frac{dr}{r}\right)\left(\int_{-1}^1 (\frac{d}{d\theta}\tilde{\varphi}_\delta)^2 \, d\theta\right) \\
&\lesssim \epsilon + \frac{\epsilon|\ln\lambda|}{\lambda}\frac{1}{\delta|\ln\delta|} \;=\; o(\frac{1}{|\ln\epsilon|}),
\end{aligned}$$

where we have used that $\arcsin t \le 2t$ for $t \in (0,1)$.

In D_3, we have

$$|\nabla m_\epsilon|^2 \;=\; |\nabla\Phi_\epsilon|^2 \overset{(48)}{\lesssim} \frac{1}{\lambda^2}\left(\Phi_\epsilon(\lambda,\theta)^2 + 1 + \frac{(\frac{d}{d\theta}\tilde{\varphi}_\delta)^2(\frac{\theta-\frac{\pi}{2}}{\arcsin\lambda})}{\arcsin^2\lambda}\right),$$

which implies by Lemma 3.3 that

$$\begin{aligned}
\epsilon \int_{D_3} |\nabla m_\epsilon|^2 \, dx &\lesssim \epsilon \int_0^\lambda \frac{r\,dr}{\lambda^2} + \frac{\epsilon}{\arcsin\lambda}\int_0^\lambda \frac{r\,dr}{\lambda^2}\int_{-1}^1 (\frac{d}{d\theta}\tilde{\varphi}_\delta)^2 \, d\theta \\
&\lesssim \epsilon + \frac{\epsilon}{\lambda}\frac{1}{\delta|\ln\delta|} \;=\; o(\frac{1}{|\ln\epsilon|}).
\end{aligned}$$

Step 3. Stray-field energy estimate. The stray field potential $U_\epsilon : \mathbb{R}^3 \to \mathbb{R}$, generated by the volume charges $(\nabla \cdot m_\epsilon)\mathbb{1}_{B^2}$, is defined in (2) as the solution of

$$\int_{\mathbb{R}^3} (\nabla, \frac{\partial}{\partial z})U_\epsilon \cdot (\nabla, \frac{\partial}{\partial z})\zeta \; dxdz \;=\; \int_{B^2} \nabla \cdot m_\epsilon \; \zeta \; dx, \qquad \text{for all } \zeta \in C_c^\infty(\mathbb{R}^3).$$

The existence and uniqueness of this solution are a direct consequence of Lax–Milgram's Theorem and are proved in Appendix. By an approximation argument, the above equation holds for all $\zeta \in \dot{H}^1(\mathbb{R}^3)$. In particular by choosing $\zeta = U_\epsilon$ we have

$$\int_{\mathbb{R}^3} |(\nabla, \frac{\partial}{\partial z})U_\epsilon|^2 \; dxdz \;=\; \int_{B^2} \nabla \cdot m_\epsilon \; U_\epsilon \; dx. \tag{50}$$

In order to estimate the stray field energy, we will estimate the right hand side of (50) in the three subdomains $B^2 \;=\; D_1 \cup D_2 \cup D_3$. We first note that

$$\int_{D_1} \nabla \cdot m_\epsilon \; U_\epsilon \; dx \;=\; 0. \tag{51}$$

For the estimate in D_2, we compute in polar coordinates

$$\nabla \cdot m_\epsilon \;=\; -m_\epsilon^\perp \cdot \nabla \Phi_\epsilon \overset{(47)}{=} \; \frac{v_\epsilon}{r} - \frac{du_\epsilon}{d\theta} \cdot \frac{1}{r}$$

for every $(\theta, r) \in D_2$. By Hölder's inequality and Sobolev's embedding theorem, we estimate

$$\begin{aligned}
\left| \int_{D_2} U_\epsilon \frac{v_\epsilon}{|x|} \; dx \right| &\leq \left(\int_{D_2} U_\epsilon^4 \; dx \right)^{1/4} \left(\int_{D_2} |\frac{\sin \varphi_\epsilon}{r}|^{4/3} \; dx \right)^{3/4} \\
&\leq \left(\int_{\mathbb{R}^2} U_\epsilon^4 \; dx \right)^{1/4} \left(\int_\lambda^1 \int_{\frac{\pi}{2} - \arcsin\frac{\lambda}{r}}^{\frac{\pi}{2} + \arcsin\frac{\lambda}{r}} |\sin \varphi_\epsilon(\theta)|^{4/3} \; d\theta \frac{dr}{r^{1/3}} \right)^{3/4} \\
&\lesssim \|U_\epsilon\|_{\dot{H}^{1/2}(\mathbb{R}^2)} \left(\arcsin\lambda \int_\lambda^1 \int_{-1}^1 |\sin \tilde{\varphi}_\delta(s)|^{4/3} \; ds \frac{dr}{r^{1/3}} \right)^{3/4} \\
&\lesssim \lambda^{3/4} \|U_\epsilon\|_{\dot{H}^1(\mathbb{R}^3)} \;=\; O(\frac{1}{|\ln \epsilon|^{3/2}}) \|U_\epsilon\|_{\dot{H}^1(\mathbb{R}^3)}.
\end{aligned} \tag{52}$$

Integration by parts leads to:

$$\begin{aligned}
\left| \int_{D_2} U_\epsilon \frac{du_\epsilon}{d\theta} \frac{dx}{|x|} \right| \;&=\; \left| \int_\lambda^1 \int_{S^1} U_\epsilon \frac{du_\epsilon}{d\theta} \; d\sigma(\theta) dr \right| \;=\; \left| \int_\lambda^1 \int_{S^1} u_\epsilon \frac{dU_\epsilon(r, \cdot)}{d\theta} \; d\sigma(\theta) dr \right| \\
&\leq \int_0^1 \|u_\epsilon\|_{\dot{H}^{1/2}(\mathbb{R})} \|U_\epsilon(r, \cdot)\|_{\dot{H}^{1/2}(S^1)} \; dr.
\end{aligned}$$

Hence, by application of Lemma 3.3 (with $\beta = 2$) and in view of (21), we obtain

$$\begin{aligned}
\left| \int_{D_2} U_\epsilon \frac{du_\epsilon}{d\theta} \frac{dx}{|x|} \right| &\leq \sqrt{\frac{4\pi + o(1)}{|\ln \epsilon|}} \int_0^1 \left(\frac{1}{2} \int_{\{|x| = r\} \times \mathbb{R}} |(\nabla, \frac{\partial}{\partial z})U_\epsilon|^2(r, \theta, z) \; d\sigma(\theta) dz \right)^{1/2} \; dr \\
&\leq \sqrt{\frac{2\pi + o(1)}{|\ln \epsilon|}} \|U_\epsilon\|_{\dot{H}^1(\mathbb{R}^3)}.
\end{aligned}$$

Together with (52), it follows that

$$\left| \int_{D_2} \nabla \cdot m_\epsilon \; U_\epsilon \; dx \right| \leq \; \sqrt{\frac{2\pi + o(1)}{|\ln \epsilon|}} \; \|U_\epsilon\|_{\dot{H}^1(\mathbb{R}^3)}. \tag{53}$$

The contribution of the stray field energy in D_3 is of lower order as we will show in the following. We express $m_\epsilon = e^{i\Phi_\epsilon}$ in polar coordinates:

$$m_\epsilon(r,\theta) \;=\; \sin(\theta-\Phi_\epsilon+\frac{\pi}{2})\vec{r}+\cos(\theta-\Phi_\epsilon+\frac{\pi}{2})\vec{\theta}, \qquad\qquad \text{for } (r,\theta)\in D_3. \tag{54}$$

Continuing to use polar coordinates, the formula $\nabla\cdot m_\epsilon = -m^\perp\cdot\nabla\Phi_\epsilon$ yields

$$\begin{aligned}\nabla\cdot m_\epsilon &\overset{(54)}{=} \cos(\theta-\Phi_\epsilon(r,\theta)+\frac{\pi}{2})\frac{\Phi_\epsilon(\lambda,\theta)}{\lambda}-\sin(\theta-\Phi_\epsilon(r,\theta)+\frac{\pi}{2})\frac{\partial_\theta\Phi_\epsilon(r,\theta)}{r}\\ &= \frac{\cos(\theta-\Phi_\epsilon(r,\theta)+\frac{\pi}{2})\Phi_\epsilon(\lambda,\theta)}{\lambda}-\frac{\sin(\theta-\Phi_\epsilon(r,\theta)+\frac{\pi}{2})}{r}-\frac{\partial_\theta\Big(\cos(\theta-\Phi_\epsilon+\frac{\pi}{2})\Big)}{r},\end{aligned}$$

for every $(\theta,r)\in D_3$. As before, by Hölder's inequality and Sobolev's embedding theorem we estimate

$$\begin{aligned}\left|\int_{D_3}U_\epsilon\frac{\cos(\theta-\Phi_\epsilon(r,\theta)+\frac{\pi}{2})\Phi_\epsilon(\lambda,\theta)}{\lambda}\,dx\right| &\lesssim \Big(\int_{D_3}U_\epsilon^4\,dx\Big)^{1/4}\Big(\int_{D_3}\frac{1}{\lambda^{4/3}}\,dx\Big)^{3/4}\\ &\lesssim \lambda^{1/2}\|U_\epsilon\|_{\dot H^{1/2}(\mathbb{R}^2)} \overset{(21)}{\lesssim} \lambda^{1/2}\|U_\epsilon\|_{\dot H^1(\mathbb{R}^3)} \overset{(42)}{=} O(\frac{1}{|\ln\epsilon|})\|U_\epsilon\|_{\dot H^1(\mathbb{R}^3)}\end{aligned} \tag{55}$$

and similarly,

$$\begin{aligned}\left|\int_{D_3}U_\epsilon\frac{\sin(\theta-\Phi_\epsilon(r,\theta)+\frac{\pi}{2})}{r}\,dx\right| &\lesssim \Big(\int_{D_3}U_\epsilon^4\,dx\Big)^{1/4}\Big(\int_{D_3}\frac{1}{r^{4/3}}\,dx\Big)^{3/4}\\ &\lesssim \lambda^{1/2}\|U_\epsilon\|_{\dot H^{1/2}(\mathbb{R}^2)} \overset{(42)}{=} O(\frac{1}{|\ln\epsilon|})\|U_\epsilon\|_{\dot H^1(\mathbb{R}^3)}.\end{aligned} \tag{56}$$

Integration by parts yields:

$$\begin{aligned}\left|\int_{D_3}U_\epsilon\,\partial_\theta\Big(\cos(\theta-\Phi_\epsilon+\frac{\pi}{2})\Big)\frac{dx}{|x|}\right| &= \left|\int_0^\lambda\int_{S^1}\cos(\theta-\Phi_\epsilon+\frac{\pi}{2})\frac{dU_\epsilon(r,\cdot)}{d\theta}\,d\sigma(\theta)dr\right|\\ &\le \int_0^\lambda\|\cos(\theta-\Phi_\epsilon+\frac{\pi}{2})\|_{\dot H^{1/2}(S^1)}\|U_\epsilon(r,\cdot)\|_{\dot H^{1/2}(S^1)}\,dr.\end{aligned} \tag{57}$$

We next estimate the homogeneous $\dot H^{1/2}-$seminorm of the $2\pi-$periodic function

$$\theta\mapsto f_r(\theta)=\cos(\theta-\Phi_\epsilon(r,\theta)+\frac{\pi}{2})$$

for $r\in(0,\lambda)$. By (45), (47) and (48), we deduce that f_r is symmetric with respect to $\pi/2$. Therefore, considering the $2\pi-$periodic potential $V_r(\theta,z)$ in θ for $r\in(0,\lambda)$,

$$V_r(\theta,z) \;=\; \begin{cases} f_r(\sqrt{(\theta-\frac{\pi}{2})^2+z^2}+\frac{\pi}{2}) & \text{if } (\theta-\frac{\pi}{2})^2+z^2\in(0,\pi^2),\\ f_r(3\pi/2) & \text{if } (\theta-\frac{\pi}{2})^2+z^2>\pi^2 \text{ and } \theta\in(-\pi/2,3\pi/2),\end{cases}$$

by (47) and (48), we compute

$$\begin{aligned}\|\cos(\theta-\Phi_\epsilon-\frac{3\pi}{2})\|^2_{\dot H^{1/2}(S^1)} &\overset{(21)}{\lesssim} \int_{-\pi/2}^{3\pi/2}\int_{\mathbb{R}}|\nabla V_r|^2\,d\theta dz \;\lesssim\; \int_0^\pi s\Big|\frac{df_r}{ds}(s+\frac{\pi}{2})\Big|^2\,ds\\ &\lesssim \int_0^\pi s\bigg((1-r/\lambda)^2+(r/\lambda)^2(\frac{1}{\arcsin\lambda}\frac{d\tilde\varphi_\delta}{d\theta}(\frac{s}{\arcsin\lambda}))^2\bigg)\,ds\\ &\lesssim (1-r/\lambda)^2+(r/\lambda)^2\int_0^\infty t(\frac{d\tilde\varphi_\delta}{dt})^2\,dt\\ &\lesssim 1+\int_0^\infty t(\frac{d\tilde\varphi_\delta}{dt})^2\,dt,\end{aligned}$$

since $r < \lambda$ in D_3. In view of definition (43), we obtain:

$$\int_0^\infty t(\frac{d\tilde{\varphi}_\delta}{dt})^2\ dt \overset{(43)}{\lesssim} \int_{\{\sqrt{\frac{1}{4}-\delta^2}\leq\ |t|\leq 1\}} t|\frac{d}{dt}\tilde{\theta}_\delta|^2 + \int_{\{|t|\leq\sqrt{\frac{1}{4}-\delta^2}\}} \frac{t}{w_\delta(1-w_\delta)}|\frac{d}{dt}w_\delta|^2.$$

For the first term of the RHS, we have

$$|\frac{d}{dt}\tilde{\theta}_\delta| \overset{(44)}{=} \frac{\arccos\frac{|\ln 4\delta|}{|\ln\delta|}}{1-\sqrt{\frac{1}{4}-\delta^2}} \lesssim \sqrt{1-\frac{|\ln 4\delta|}{|\ln\delta|}} \lesssim \frac{1}{|\ln\delta|^{1/2}} \quad \text{for } t\in(\sqrt{\frac{1}{4}-\delta^2},1).$$

Hence,

$$\int_{\{\sqrt{\frac{1}{4}-\delta^2}\leq|t|\leq 1\}} t|\frac{d}{dt}\tilde{\theta}_\delta|^2 \lesssim \frac{1}{|\ln\delta|} = O(\frac{1}{|\ln\epsilon|}) \quad \text{as } \epsilon\to 0.$$

For the second term of the RHS, we obtain after the change of variables $t=\delta s$:

$$\begin{aligned}\int_{\{|t|\leq\sqrt{\frac{1}{4}-\delta^2}\}} \frac{t}{w_\delta(1-w_\delta)}|\frac{d}{dt}w_\delta|^2\ dt &\overset{(33)}{\lesssim} \int_0^{1/2} \frac{t^3}{(t^2+\delta^2)^2\ln\frac{t^2+\delta^2}{\delta^2}\ln\frac{1}{t^2+\delta^2}}\ dt\\ &\lesssim \int_0^{\frac{1}{2\delta}} \frac{s^2}{(s^2+1)^2(\ln\frac{1}{\delta^2}-\ln(s^2+1))\ln(s^2+1)}\ ds\\ &\lesssim \frac{1}{|\ln\delta|}+\frac{\ln|\ln\delta|}{|\ln\delta|}+\ln|\ln\delta| = O(\ln|\ln\delta|)\end{aligned}$$

where the three estimates follow from the splitting of the last integral into the three intervals $(0,1)$, $(1,|\ln\delta|)$ and $(|\ln\delta|,\frac{1}{2\delta})$, respectively. We conclude that

$$\|\cos(\theta-\Phi_\epsilon-\frac{3\pi}{2})\|^2_{\dot{H}^{1/2}(S^1)} \lesssim \ln|\ln\delta|.$$

In view of (57) and (21), this yields

$$\begin{aligned}\left|\int_{D_3} U_\epsilon\partial_\theta\Big(\cos(\theta-\Phi_\epsilon+\frac{\pi}{2})\Big)\frac{dx}{|x|}\right| &\lesssim \sqrt{\ln|\ln\delta|}\int_0^\lambda\left(\int_{\{|x|=r\}\times\mathbb{R}}|(\nabla,\frac{\partial}{\partial z})U_\epsilon|^2(r,\theta,z)\ d\sigma(\theta)dz\right)^{1/2} dr\\ &\leq \sqrt{\lambda\ln|\ln\delta|}\|U_\epsilon\|_{\dot{H}^1(\mathbb{R}^3)} = O(\frac{(\ln|\ln\epsilon|)^{1/2}}{|\ln\epsilon|})\|U_\epsilon\|_{\dot{H}^1(\mathbb{R}^3)}.\end{aligned}$$

By (55) and (56), we get

$$\left|\int_{D_3} \nabla\cdot m_\epsilon U_\epsilon\ dx\right| = O(\frac{(\ln|\ln\epsilon|)^{1/2}}{|\ln\epsilon|})\ \|U_\epsilon\|_{\dot{H}^1(\mathbb{R}^3)}. \tag{58}$$

The estimates (51), (53) and (58) together yield

$$\int_{\mathbb{R}^3}|(\nabla,\frac{\partial}{\partial z})U_\epsilon|^2\ dxdz \overset{(50)}{=} \int_{B^2}\nabla\cdot m_\epsilon\ U_\epsilon\ dx \leq \sqrt{\frac{2\pi+o(1)}{|\ln\epsilon|}}\ \|U_\epsilon\|_{\dot{H}^1(\mathbb{R}^3)},$$

which concludes the estimate for the stray field energy and hence the proof of the proposition. □

4.2 Lower bound

In the following we give the proof for the lower bound in Theorem 1.3. The proof combines a dynamical system argument with the interpolation inequality in Lemma 2.2.

Proof of Theorem 1.3. Without loss of generality, we may assume that all $m_\epsilon : B^2 \to S^1$ are smooth since smooth maps with values into S^1 are dense in $H^1(B^2, S^1)$ and furthermore, we may also assume that

$$E_\epsilon^{loc}(m_\epsilon, h_\epsilon) \;\leq\; 2\pi \qquad\qquad \text{as } \epsilon \to 0. \tag{59}$$

We divide our proof in several steps:

Step 1. A dynamical system argument. Crucial for the estimate of the lower bound is the control of the stray field energy. Since the stray field energy is created by $\nabla \cdot m_\epsilon$, by Stokes theorem this implies a control for the net flow of m_ϵ across the boundary of any subdomain of B^2. The first step of the proof consists of finding such a domain with maximal net flow. Using Stokes theorem, this eventually yields the optimal lower bound for the energy. As in [6, 17], we consider the flow generated by the rotated vector field $m_\epsilon^\perp$ (see Figure 10). In particular, let γ_ϵ be the orbit passing through the origin, defined by

$$\dot\gamma_\epsilon(t) \;=\; m_\epsilon^\perp(\gamma_\epsilon(t)), \qquad\qquad \gamma_\epsilon(0) \;=\; 0. \tag{60}$$

Since $m_\epsilon^\perp$ is smooth and unit–valued in B^2, the orbit cannot have cycles, but rather has to enter and leave every ball $B \subset B^2$ in finite time. Indeed, if m_ϵ would form a cycle, then m_ϵ would have a degree 1 on the cycle, so m_ϵ would have a zero inside which is not possible since $|m_\epsilon| = 1$.

Figure 10: Construction of γ_ϵ, χ_ϵ and γ_ϵ^+

We will show that for arbitrary fixed $0 < \delta < 1$, we have

$$E_\epsilon^{loc}(m_\epsilon, h_\epsilon) \;\geq\; 2\pi - C\delta - o_\delta(1) \qquad\qquad \text{as } \epsilon \to 0, \tag{61}$$

where C is a universal constant, in particularly independent on ϵ and δ. The Landau symbol $o_\delta(1)$ corresponds to a function that converges to zero for $\epsilon \to 0$ for every fixed $\delta > 0$ (the convergence hence may depend on δ). Note that the statement of the proposition follows from (61).

We first introduce some notation: It is convenient to work in polar coordinates (r, θ). Furthermore we denote by $\vec r$ (resp. $\vec\theta$) the unit vector in radial (resp. angular) direction. Let $B_r \subseteq B^2$ denote the ball with radius r around the origin and let $A_{r_1}^{r_2} := B_{r_2} \backslash B_{r_1}$ be the annulus enclosed by the radii r_1 and r_2.

The following observation is crucial for the proof: We have that the length $\mathcal{H}^1(\gamma_\epsilon)$ of the orbit γ_ϵ is bounded by below by

$$\mathcal{H}^1(\gamma_\epsilon) \;\geq\; 2. \tag{62}$$

This follows, since γ_ϵ has to leave and enter every ball $B_r \subset B^2$ with $r < 1$ at two different points (in between passing through the origin). In fact, γ_ϵ divides B^2 into two domains $\Omega_\pm$. We choose $\Omega_\pm$ such that the flow of m_ϵ passing through γ_ϵ flows from Ω_+ to Ω_- (see Figure 10). We introduce the indicator function χ_ϵ by

$$\chi_\epsilon(x) \;=\; \pm 1 \qquad\qquad \text{on } \Omega_\pm.$$

Therefore, we have

$$|\nabla \chi_\epsilon| = -\nabla \chi_\epsilon \cdot m_\epsilon = 2\mathcal{H}^1 \lfloor \{\gamma_\epsilon\}.$$

In Step 2, we prove that the length of the orbits are uniformly bounded in the interior of B^2. Then in Step 3, we demonstrate the idea of the proof with a 'naive' attempt. This first attempt fails by a factor of 2. By a more refined analysis using a localization argument we then obtain the optimal constant for the lower bound of the energy in Steps 4 and 5.

Step 2. Locally uniform bounds on the orbit length. We first show that the total length of γ_ϵ (i.e., the jump set of χ_ϵ) is bounded in every interior ball $B_{1-2\delta^3}$ for ϵ sufficiently small: We claim that there is a constant only depending on δ such that

$$\|\nabla \chi_\epsilon\|_{\mathcal{M}(B_{1-2\delta^3})} \;\le\; C_\delta. \tag{63}$$

We follow the lines in [17]. Let $\tilde{\chi}_\epsilon := \chi_\epsilon \mathbb{1}_{B_{1-2\delta^3}}$. We first note that

$$\|\nabla \chi_\epsilon\|_{\mathcal{M}(B_{1-2\delta^3})} \;\le\; \|\nabla \tilde{\chi}_\epsilon\|_{\mathcal{M}(B^2)} + 2\pi.$$

Hence in order to obtain (63), it is enough to show

$$\|\nabla \tilde{\chi}_\epsilon\|_{\mathcal{M}(B^2)} \;\le\; C_\delta. \tag{64}$$

Choose a smooth cut–off function $0 \le \eta \le 1$ with $\eta = 1$ on $B_{1-2\delta^3}$, $\eta = 0$ outside $B_{1-\delta^3}$ and $\|\nabla \eta\|_{C^0} \le C_\delta$. We apply the local interpolation inequality (Lemma 2.2) for $\tilde{\chi}_\epsilon$ and η. Then by (59), we get

$$\left| \int_{B^2} \tilde{\chi}_\epsilon \; \nabla \cdot m_\epsilon \; dx \right| \;\le C \|\nabla \tilde{\chi}_\epsilon\|^{1/2}_{\mathcal{M}(B^2)} + \frac{C_\delta (1 + \|\nabla \tilde{\chi}_\epsilon\|_{\mathcal{M}(B^2)})}{|\ln \epsilon|^{1/2}}.$$

Integration by parts on the left hand side combined with (60) yields

$$\|\nabla \tilde{\chi}_\epsilon\|_{\mathcal{M}(B^2)} - C \;\le C \|\nabla \tilde{\chi}_\epsilon\|^{1/2}_{\mathcal{M}(B^2)} + \frac{C_\delta (1 + \|\nabla \tilde{\chi}_\epsilon\|_{\mathcal{M}(B^2)})}{|\ln \epsilon|^{1/2}}.$$

Now, the last term on the right hand side can be absorbed by the left hand side if ϵ is sufficiently small. Then (64) and hence (63) follow easily.

Step 3. Radial cut–off and a non-optimal lower bound. We introduce a radial cut–off function

$$\eta_1 = \eta_1(r) \in C_c^\infty(A_{\delta^3}^{1-2\delta^3}) \text{ with } 0 \le \eta_1 \le 1, |\nabla \eta_1| \le C_\delta \text{ and } \eta_1 = 1 \text{ in } A := A_{2\delta^3}^{1-3\delta^3}.$$

Note that at this point of the proof, the cut–off near the origin is not needed. However, we use this cut–off here, since it will be needed later. We have chosen η_1 such that Step 2 applies, i.e. the orbit has bounded length on $\operatorname{supp} \eta$. Let $\gamma_{\epsilon,A}$ be the part of γ_ϵ in A. Since we have cut off only a small part in the center of the disc, the argument in (62) still yields

$$\mathcal{H}^1(\gamma_{\epsilon,A}) \;\ge\; 2 - C\delta. \tag{65}$$

The function χ_ϵ and the orbit $\gamma_{\epsilon,A}$ have been chosen such that the flow over the jump set of χ_ϵ is maximal. In fact, we have

$$2\mathcal{H}^1(\gamma_{\epsilon,A}) \;\leq\; \int_{B^2} \eta_1^2 |\nabla \chi_\epsilon| \; dx \overset{(60)}{=} \; -\int_{B^2} \eta_1^2 \; \nabla \chi_\epsilon \cdot m_\epsilon \; dx. \tag{66}$$

We prove a non-optimal lower bound where instead of the leading order constant 2π in (61) we obtain only π. For that, we apply integration by parts on the 'duality product' of χ_ϵ and $\nabla \cdot m_\epsilon$, to get

$$\int_{B^2} \eta_1^2 \; \chi_\epsilon \;\; \nabla \cdot m_\epsilon \; dx \;=\; -\int_{B^2} \eta_1^2 \; \nabla \chi_\epsilon \cdot m_\epsilon \; dx - \int_{B^2} \chi_\epsilon \nabla(\eta_1^2) \cdot m_\epsilon \; dx. \tag{67}$$

Since $\eta_1 = \eta_1(r)$ we obtain for the last term on the right hand side of (67)

$$\left| \int_{B^2} \chi_\epsilon \nabla(\eta_1^2) \;\cdot m_\epsilon \; dx \right| \;\leq\; \int_{B^2} \left| \partial_r(\eta_1^2) \; m_\epsilon \cdot \vec{r} \right| \; dx \;\overset{(4)}{=}\; o_\delta(1) \quad \text{as } \epsilon \to 0. \tag{68}$$

Inequalities (66), (67) and (68) together yield

$$\int_{B^2} \eta_1^2 \; \chi_\epsilon \;\; \nabla \cdot m_\epsilon \; dx \;\geq\; \|\eta_1^2 \nabla \chi_\epsilon\|_{\mathcal{M}(B^2)} - o_\delta(1) \quad \text{as } \epsilon \to 0. \tag{69}$$

Application of Lemma 2.2 yields

$$\begin{aligned} \left| \int_{B^2} \eta_1^2 \; \chi_\epsilon \;\; \nabla \cdot m_\epsilon \; dx \right| \;&\leq\; \left(\frac{4}{\pi} \|\chi_\epsilon\|_{L^\infty(B^2)} \|\eta_1^2 \nabla \chi_\epsilon\|_{\mathcal{M}(B^2)} \; E_\epsilon^{loc}(m_\epsilon, h_\epsilon) \right)^{1/2} \\ &\qquad + \frac{C(1 + \|\nabla \eta_1\|_{C^0})(1 + \|\eta_1 \nabla \chi_\epsilon\|_{\mathcal{M}(B^2)})}{|\ln \epsilon|^{1/2}} \\ &\overset{(63)}{\leq}\; \left(\frac{4}{\pi} \|\eta_1^2 \nabla \chi_\epsilon\|_{\mathcal{M}(B^2)} \; E_\epsilon^{loc}(m_\epsilon, h_\epsilon) \right)^{1/2} + o_\delta(1) \quad \text{as } \epsilon \to 0. \end{aligned}$$

In view of (69), this turns into

$$\|\eta_1^2 \nabla \chi_\epsilon\|_{\mathcal{M}(B^2)} \;\leq\; \left(\frac{4}{\pi} \; \|\eta_1^2 \nabla \chi_\epsilon\|_{\mathcal{M}(B^2)} \; E_\epsilon^{loc}(m_\epsilon, h_\epsilon) \right)^{1/2} + o_\delta(1).$$

Using (59), (65) and (66), this implies

$$E_\epsilon^{loc}(m_\epsilon, h_\epsilon) \geq \; \frac{\pi \|\eta_1^2 \nabla \chi_\epsilon\|_{\mathcal{M}(B^2)}}{4} + o_\delta(1) \;\overset{(66)}{\geq}\; \frac{\pi \mathcal{H}^1_\epsilon(\gamma_{\epsilon,A})}{2} + o_\delta(1) \;\overset{(65)}{\geq}\; \pi - C\delta + o_\delta(1).$$

We conclude that this first attempt of proof misses the optimal constant 2π by a factor of 2. Note that as a side result of this paragraph, the last inequality together with (59) yields

$$\mathcal{H}^1(\gamma_{\epsilon,A}) \;\leq\; 4 + o_\delta(1), \tag{70}$$

which is a substantial improvement with respect to (63), but still not optimal since in the limit $\epsilon \to 0$, we expect the length of the orbit γ_ϵ to be close to 2.

Step 4. Radial and angular cut–off. The optimal lower bound in a special case. In this paragraph, we give an argument providing the optimal constant, but in a restricted setting. In contrary to before, the argument is solely based on the part γ_ϵ^+ of γ_ϵ before the curve passes the origin (see Figure 11). In fact, only on this part of the orbit the magnetization (generically) points opposite to

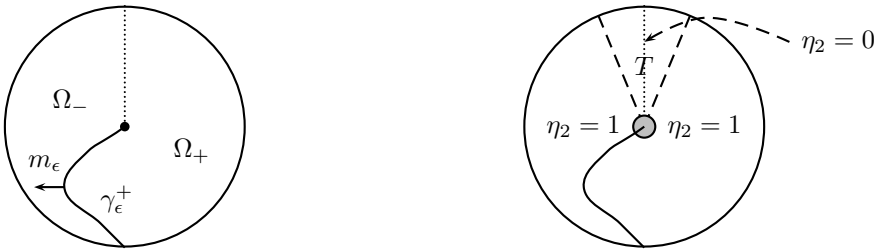

Figure 11: Angular cut–off function η_2

the limiting vortex configuration $x^\perp/|x|$. Reparametrizing the orbits, we assume in the following that all orbits γ_ϵ enter the disc B^2 at time $t = 0$. Furthermore, by rotational invariance of the energy, we may assume without loss of generality that all γ_ϵ enter 'at the bottom' of B^2 (in polar coordinates this corresponds to $(r, \theta) = (1, \frac{3}{2}\pi)$) at time $t = 0$.

We consider here the special case where we have a uniform control on the rotation around the origin: We assume that the sector

$$T \;=\; \{(r,\theta) : |\theta - \pi/2| < \pi/8\} \tag{71}$$

is not touched by any γ_ϵ^+ for all $\epsilon > 0$, see Figure 11. Let $\eta_1 = \eta_1(r)$ be the same cut–off function as in Step 3. Furthermore let $\eta_2 = \eta_2(\theta)$, independent of ϵ, such that $\eta_2 = 1$ outside T, $\eta_2 = 0$ at $\theta = \pi/2$ and

$$\eta = \eta_1\eta_2 \in C_c^\infty(B^2) \quad \text{with} \quad 0 \le \eta \le 1, \quad |\nabla\eta| \le C_\delta \text{ in } B^2,$$

where η_1 is the cut-off function defined in Step 3. The domains $\Omega_\pm$ are defined slightly different than before: The curve γ_ϵ^+ and the semi-line $\theta = \pi/2$ divide the disc into two parts. We denote these two parts by $\Omega_\pm$. As before, Ω_+ is chosen such that the flow of m_ϵ crossing through γ_ϵ^+ is directed from Ω_+ to Ω_- and we define the indicator function χ_ϵ by $\chi_\epsilon(x) = \pm 1$ on $\Omega_\pm$. By our choice of η, we have

$$-\int_{B^2} \eta^2 \; \nabla\chi_\epsilon \cdot m_\epsilon \; dx \;=\; \|\eta^2\nabla\chi_\epsilon\|_{\mathcal{M}(B^2)} \quad \text{and} \quad \|\eta^2\nabla\chi_\epsilon\|_{\mathcal{M}(B^2)} \;\ge\; 2\mathcal{H}^1(\gamma_\epsilon^+) - C\delta \;\ge\; 2 - C\delta. \tag{72}$$

As before, we apply integration by parts:

$$\int_{B^2} \eta^2 \; \chi_\epsilon \; \nabla\cdot m_\epsilon \; dx \;=\; -\int_{B^2} \eta^2 \; \nabla\chi_\epsilon \cdot m_\epsilon \; dx - \int_{B^2} \nabla(\eta^2) \; \chi_\epsilon \cdot m_\epsilon \; dx. \tag{73}$$

For the last term on the right hand side of (73), we get using the definitions of χ and η:

$$\begin{aligned}
-\int_{B^2} \nabla(\eta^2) \; \chi_\epsilon \cdot m_\epsilon \; dx \;&=\; -\int_{B^2} \frac{1}{r}\partial_\theta(\eta^2) \; \chi_\epsilon \; m_\epsilon \cdot \vec{\theta} \; dx - \int_{B^2} \partial_r(\eta^2) \; \chi_\epsilon \; m_\epsilon \cdot \vec{r} \; dx \\
&\overset{(4)}{=} \; -\int_0^1 \int_{\pi/4}^{\pi/2} \partial_\theta(\eta_2^2)\eta_1^2 \; d\theta dr + \int_0^1 \int_{\pi/2}^{3\pi/4} \partial_\theta(\eta_2^2)\eta_1^2 \; d\theta dr + o_\delta(1) \\
&=\; \big(\eta_2^2(\pi/4) - 2\eta_2^2(\pi/2) + \eta_2^2(3\pi/4)\big) \int_0^1 \eta_1^2 \; dr + o_\delta(1) \\
&\ge\; 2 - C\delta + o_\delta(1).
\end{aligned} \tag{74}$$

Applying (72) and (74) on the right hand side of (73) yields

$$\int_{B^2} \eta^2 \ \chi_\epsilon \ \nabla\cdot m_\epsilon \ dx \ \geq \ \ \|\eta^2 \nabla \chi_\epsilon\|_{\mathcal{M}(B^2)} + 2 - C\delta + o_\delta(1). \tag{75}$$

On the other hand, the interpolation estimate in Lemma 2.2 yields

$$\left| \int_{B^2} \eta^2 \ \chi_\epsilon \ \nabla\cdot m_\epsilon \ dx \right| \overset{(63)}{\leq} \ \ \left(\frac{4}{\pi} \|\chi_\epsilon\|_{L^\infty(B^2)} \|\eta^2 \nabla \chi_\epsilon\|_{\mathcal{M}(B^2)} \ E_\epsilon^{loc}(m_\epsilon, h_\epsilon) \right)^{1/2} + o_\delta(1).$$

Together with (75), this implies

$$\|\eta^2 \nabla \chi_\epsilon\|_{\mathcal{M}(B^2)} + 2 \ \leq \ \left(\frac{4}{\pi} \|\eta^2 \nabla \chi_\epsilon\|_{\mathcal{M}(B^2)} \ E_\epsilon^{loc}(m_\epsilon, h_\epsilon) \right)^{1/2} + C\delta + o_\delta(1).$$

It follows that (also using (59) and (72))

$$E_\epsilon^{loc}(m_\epsilon, h_\epsilon) \ \geq \ \ \frac{\pi(\|\eta^2 \nabla \chi_\epsilon\|_{\mathcal{M}(B^2)} + 2)^2}{4\|\eta^2 \nabla \chi_\epsilon\|_{\mathcal{M}(B^2)}} - C\delta + o_\delta(1) \ \geq \ 2\pi - C\delta + o_\delta(1),$$

thus yielding the optimal constant 2π. Note that in the last inequality we used that $\varphi(t) = (t+2)^2/t$ achieves its minimum on $(0, +\infty)$ for $t = 2$.

Step 5: Localization argument. General case. It remains to generalize the above argument for arbitrary orbits γ_ϵ^+. In general, each orbit γ_ϵ^+ can rotate many times about the origin. However, this goes along with an increase of length of γ_+ which in turn yields a better control on the energy. Using a localization argument and by balancing these two effects (rotation & length of γ_ϵ^+), we obtain the optimal constant for the lower bound of the energy. We control the rotation in terms of annuli of fixed thickness (depending on δ). We again use the parameter $\delta > 0$ as 'cut–off' around the origin (in order to prevent infinitely many rotations near zero) and near ∂B^2 (in order to be able to apply the localized interpolation inequality). We inductively define

$$r_0 \ = \ 1 \qquad\qquad \text{and} \qquad\qquad r_{k+1} \ = \ (1-\delta) r_k, \tag{76}$$

i.e., $r_k = (1-\delta)^k$, $k \geq 0$. After finitely many iterations $N = N_\delta$ we have $r_N \leq \ \delta < r_{N-1}$. We define the annuli

$$A_k \ := \ \big\{ (r, \theta) \ : \ r_k \leq r \leq r_{k-1} \big\} \qquad\qquad \text{for} \qquad\qquad 1 \leq \ k \leq \ N-1$$

and $A_N := B_{r_N}$. Furthermore, let $s_{\epsilon,k}$ be the time t when $\gamma_\epsilon^+(t)$ (with starting point on ∂B^2) first touches the circle $\{r = r_{k-1} - \delta^3\}$ and let $t_{\epsilon,k}$ be the time when the curve touches the circle $\{r = r_k + \delta^3\}$ the last time before passing through the origin. Furthermore, let $\gamma_{\epsilon,k}^+ : (s_{\epsilon,k}, t_{\epsilon,k}) \to B^2$ the corresponding restriction of γ_ϵ^+. The above definitions mean that $\gamma_{\epsilon,k}^+$ roughly (up to a δ^3–misfit) connects the outer and inner boundary of A_k. We distinguish between 'good' and 'bad' annuli according to the rotation about the origin that $\gamma_{\epsilon,k}^+$ assumes within A_k: For this, using polar coordinates we define $\Theta_{\epsilon,k} \in [0, 2\pi]$ by

$$\Theta_{\epsilon,k} \ := \ \left| \left\{ \theta \in [0, 2\pi) : \theta \text{ is attained by } \gamma_{\epsilon,k}^+ \right\} \right|.$$

Here and in the following, we will always think as $\epsilon \to 0$ in terms of a sequence $\epsilon_j \to 0$. For the sake of simplicity, we skip the index j. By possibly taking a subsequence (and in view of (63)) we

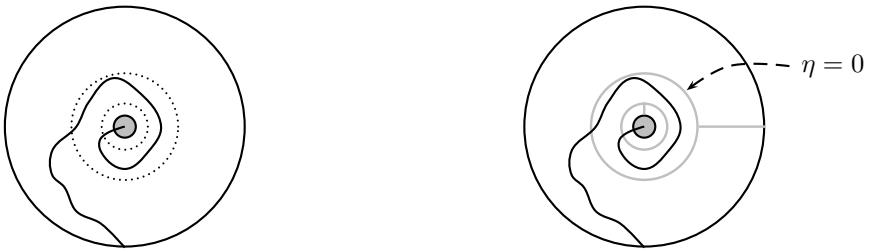

Figure 12: Localization argument

may assume that $t_{\epsilon,k} \to t_k$, $s_{\epsilon,k} \to s_k$ and $\Theta_{\epsilon,k} \to \Theta_k$ as $\epsilon \to 0$. We consider A_k to be a 'good' annulus for the sequence $\{m_\epsilon\}$, if the rotation of the orbit is controlled, i.e.

$$|\Theta_k| \leq \frac{3}{2}\pi. \tag{77}$$

In this case, there is a $\theta_{\epsilon,k}$ and a sector

$$T_{\epsilon,k} \;=\; A_k \cap \{(r,\theta) : |\theta - \theta_{\epsilon,k}| < \pi/8\}$$

which is not touched by $\gamma^+_{\epsilon,k}$ for small $\epsilon > 0$. By possibly taking a subsequence we may assume that $\theta_{\epsilon,k} \to \theta_k$ as $\epsilon \to 0$.

For each ϵ, the orbit γ^+_ϵ separates the annulus $B_{1-\delta^3} \setminus B_\delta$ into two parts. As in Step 1 of the proof, we define $\chi_\epsilon : B^2 \to \{\pm 1\}$ such that

$$\nabla \chi_\epsilon = -2m_\epsilon \mathcal{H}^1 \lfloor \{\gamma^+_\epsilon\} \qquad\qquad \text{in } \; B_{1-\delta^3} \setminus \overline{B_\delta}$$

and we set $\chi_\epsilon = 0$ in $B_\delta \cup (B^2 \setminus B_{1-\delta^3})$. We now define an ϵ–independent cut–off function η that serves two purposes: It localizes the estimate onto each single annulus. Secondly, if the annulus is a "good" annulus (i.e. with controlled rotation of the orbit as described before), η is used to separate the annulus onto two separate parts (as in Step 4). On the bad annuli, we will use the estimate as in Step 3. We define

$$\eta = \eta_1 \eta_2 \in [0,1] \qquad\qquad \text{with} \qquad\qquad |\nabla \eta| \leq C_\delta$$

as follows (see Figure 12): First, we choose η_1 to be radial such that $\eta_1(r) = 0$ on

$$\mathcal{N}_1 = (0,\delta) \cup (1-2\delta^3, 1) \cup \bigcup_{k=1}^{N} (r_k - \delta^3, r_k + \delta^3)$$

and $\eta_1 = 1$ outside a δ^3–neighborhood of $\mathcal{N}$. Secondly, we choose η_2 such that for every good annulus A_k, i.e., $|\Theta_k| \leq 3\pi/2$, we impose that η_2 depends only on θ and $\eta_2 = 0$ in $(\theta_k - \delta^3, \theta_k + \delta^3)$ and $\eta_2 = 1$ outside a δ^3–neighborhood of that interval. The function η_2 may jump on ∂A_k, but it doesn't affect η since $\eta_1 = 0$ around a neighborhood of ∂A_k. The number N_δ of annuli is estimated by

$$N_\delta \;\lesssim\; \frac{|\ln \delta|}{|\ln(1-\delta)|} \;\leq\; \frac{1}{\delta^2}. \tag{78}$$

In particular, the area of the δ^3–neighborhood of $\mathcal{N}$ is estimated by $C\delta$.

On each 'good' annulus A_k, the arguments in Step 4 of the proof show that we have a good lower bound for the duality product:

$$\int_{A_k} \eta^2 \ \chi_\epsilon \ \nabla\cdot m_\epsilon \ dx \ \geq \ \|\eta^2 \nabla \chi_\epsilon\|_{\mathcal{M}(A_k)} + 2(r_k - r_{k+1}) - C\delta^3 - o_\delta(1). \tag{79}$$

Indeed, (79) correponds to (75) when adjusting the cut–off function η from the annulus considered in Step 4 to the annulus A_k considered here. However, we only have weak control on the length of the corresponding orbit

$$\|\eta^2 \nabla \chi_\epsilon\|_{\mathcal{M}(A_k)} \ \geq \ 2(r_k - r_{k+1}) - C\delta^3. \tag{80}$$

Note that the factor 2 on the right hand side of the above estimate relates to the fact that χ_ϵ has a jump of size 2 over γ_ϵ^+. Now, let us assume that (77) is not fulfilled for the annulus A_k, i.e., it is a bad annulus. Then the arguments in step 3 of the proof only give us a weaker lower bound on the duality product:

$$\int_{A_k} \eta^2 \ \chi_\epsilon \ \nabla\cdot m_\epsilon \ dx \ \geq \ \|\eta^2 \nabla \chi_\epsilon\|_{\mathcal{M}(A_k)} - C\delta^3 - o_\delta(1). \tag{81}$$

Indeed, (81) correponds to (69) when adjusting the cut–off function η from the annulus considered in step 4 to the annulus A_k considered here. However, in view of $\Theta_k > \frac{3}{2}$, we have a better lower bound on the length of the corresponding orbit:

$$\|\eta^2 \nabla \chi_\epsilon\|_{\mathcal{M}(A_k)} \ \geq \ 2 \cdot \frac{3}{2}\pi r_k - C\delta^3 \overset{(76)}{\geq} \ \frac{3\pi}{\delta} \ (r_k - r_{k+1}) - C\delta^3. \tag{82}$$

Let $0 \leq R^{bad} \leq 1$ be defined by as the sum of the thicknesses of all annuli that do not satisfy (77) and let $R^{good} = 1 - R^{bad}$. We recall (78) and that for each annulus the thickness of the radial cut–off is less than δ^3. Summing over all orbits and using (80) and (82), we hence obtain

$$\|\eta^2 \nabla \chi_\epsilon\|_{\mathcal{M}(B^2)} \ = \ \sum_k \int_{A_k} \eta^2 |\nabla \chi_\epsilon| \ dx \ \geq \ 2R^{good} + \frac{3\pi R^{bad}}{\delta} - C\delta. \tag{83}$$

Analogously, using (79), (81) and summing over all orbits we get

$$\int_{B^2} \eta^2 \ \chi_\epsilon \ \nabla\cdot m_\epsilon \ dx \ \geq \ \|\eta^2 \nabla \chi_\epsilon\|_{\mathcal{M}(B^2)} + 2R^{good} - C\delta - o_\delta(1). \tag{84}$$

By Lemma 2.2 we have

$$\left| \int_{B^2} \eta^2 \ \chi_\epsilon \ \nabla\cdot m_\epsilon \ dx \right| \ \leq \ \left(\frac{4}{\pi} \|\chi_\epsilon\|_{L^\infty(B^2)} \|\eta^2 \nabla \chi_\epsilon\|_{\mathcal{M}(B^2)} \ E_\epsilon^{loc}(m_\epsilon, h_\epsilon) \right)^{1/2} + o_\delta(1).$$

Using (84) and since $\|\chi_\epsilon\|_{L^\infty(B^2)} = 1$, this turns into

$$\|\eta^2 \nabla \chi_\epsilon\|_{\mathcal{M}(B^2)} + 2R^{good} \ \leq \ \left(\frac{4}{\pi} \ \|\eta^2 \nabla \chi_\epsilon\|_{\mathcal{M}(B^2)} \ E_\epsilon^{loc}(m_\epsilon, h_\epsilon) \right)^{1/2} + C\delta + o_\delta(1).$$

This yields

$$\begin{aligned} E_\epsilon^{loc}(m_\epsilon, h_\epsilon) \ &\geq \ \frac{\pi(\|\eta^2 \nabla \chi_\epsilon\|_{\mathcal{M}(B^2)} + 2R^{good})^2}{4\|\eta^2 \nabla \chi_\epsilon\|_{\mathcal{M}(B^2)}} - C\delta - o_\delta(1) \\ &\overset{(83)}{\geq} \ \frac{\pi(3\pi R^{bad}/\delta + 4R^{good})^2}{4(3\pi R^{bad}/\delta + 2R^{good})} - C\delta - o_\delta(1). \end{aligned}$$

For the second inequality, we have used that $v(t) = (t + R^{good})^2/t$ is monotonically increasing in t as long as $t > R^{good}$ and also the fact that $|v(R^{good} - C\delta) - v(R^{good})| \leq C\delta$. The following simple calculation shows that we indeed get the sharp lower bound with optimal constant. Let $M := 3\pi/\delta$. Minimizing in the radius $R^{bad} \in [0, 1]$ for M large enough, we get

$$\frac{\pi(MR^{bad} + 4R^{good})^2}{4(MR^{bad} + 2R^{good})} \;=\; 2\pi\,\frac{\big((M-4)R^{bad}+4\big)^2}{8\,((M-2)R^{bad}+2)} \;\geq\; 2\pi\,\frac{M(M-4)}{(M-2)^2}.$$

(where the minimum inside $[0, 1]$ is achieved at $R^{bad} = 8/((M-2)(M-4))$ if M is large enough). It is then easy to see that for M large enough,

$$\frac{M(M-4)}{(M-2)^2} \;\geq\; 1 - \frac{C}{M} \;=\; 1 - C\delta.$$

This yields (61), thus concluding the proof of the proposition.

□

Acknowledgement. Part of this work was done during visits of R.I. at the Courant Institute, NYU, and of H.K. at Université Paris-Sud, respectively. R.I. acknowledges support from the ANR project ANR-08-BLAN-0199-01 "Micromagnetism: Mathematics Applied to New Physical Interactions" of the French Ministry of Research. H.K. would like to thank Cyrill Muratov for interesting discussions.

5 Appendix

We prove existence and uniqueness of the stray field generated by the volume charges, as well as the expression of the stray field energy. For that, we introduce the Beppo-Levi space:

$$\mathcal{BL} = \{U : \mathbb{R}^3 \to \mathbb{R} \,:\, \nabla U \in L^2(\mathbb{R}^3), \frac{U}{1+|x|} \in L^2(\mathbb{R}^3)\}.$$

Then the space $\mathcal{BL}$ endowed by the homogeneous $\dot{H}^1-$norm, i.e., $U \mapsto \|\nabla U\|_{L^2(\mathbb{R}^3)}$ is a Hilbert space and the set $C_c^\infty(\mathbb{R}^3)$ of smooth compactly supported functions is a dense set.

Theorem 5.1. *Let $m \in H^1(B^2, \mathbb{R}^2)$. Then the variational problem* (2) *has a unique solution $U_{ac} \in \mathcal{BL}$. Classically, U_{ac} satisfies*

$$\begin{cases} \Delta U_{ac} = 0 & \text{in } \mathbb{R}^3 \setminus B^2 \times \{0\}, \\ \left[\frac{\partial U_{ac}}{\partial z}\right] = -\nabla \cdot m & \text{on } B^2 \times \{0\}, \end{cases} \tag{85}$$

where $[q] = q^+ - q^-$ stands for the jump in vertical direction z of a quantity q across the horizontal plane. Moreover, the stray field energy generated by the volume charges is given by (3).

Proof. We apply Lax-Milgram's theorem for the variational problem (2) in the space $\mathcal{BL}$. For this, we only need to check that $\zeta \mapsto \int_{B^2} \nabla \cdot m\, \zeta\, dx$ is continuous as a functional in $\mathcal{BL}$. Indeed, by duality and the trace estimate, we have for every $\zeta \in \mathcal{BL}$

$$\begin{aligned} \int_{B^2} \nabla \cdot m\, \zeta(\cdot, 0)\, dx \;&\leq\; \|\nabla \cdot m\, \mathbb{1}_{B^2}\|_{\dot{H}^{-1/2}(\mathbb{R}^2)} \|\zeta(\cdot, 0)\|_{\dot{H}^{1/2}(\mathbb{R}^2)} \\ &\leq\; C\|\nabla \cdot m\, \mathbb{1}_{B^2}\|_{\dot{H}^{-1/2}(\mathbb{R}^2)} \|\nabla\zeta\|_{L^2(\mathbb{R}^3)}. \end{aligned}$$

Setting $f := \nabla \cdot m\, \mathbb{1}_{B^2}$, it remains to show that

$$\|f\|_{\dot{H}^{-1/2}(\mathbb{R}^2)} \;\leq\; C\|f\|_{L^2(\mathbb{R}^2)}, \tag{86}$$

for every $f \in L^2(\mathbb{R}^2)$ with $\operatorname{supp} f \subset B^2$. Estimate (86) can be seen as follows: Decomposing the $\dot{H}^{-1/2}(\mathbb{R}^2)-$seminorm into

$$\begin{aligned}
\|f\|^2_{\dot{H}^{-1/2}(\mathbb{R}^2)} \;&=\; \int_{|\xi|\geq 1} \frac{|\mathcal{F}(f)(\xi)|^2}{|\xi|}\, d\xi + \int_{|\xi|\leq 1} \frac{|\mathcal{F}(f)(\xi)|^2}{|\xi|}\, d\xi, \\
&\leq\; \|\mathcal{F}f\|_{L^2(\mathbb{R}^2)} + \|\mathcal{F}f\|^2_{L^\infty(\mathbb{R}^2)} \int_{|\xi|\leq 1} \frac{1}{|\xi|}\, d\xi \\
&\leq\; C\, \left(\|f\|^2_{L^2(\mathbb{R}^2)} + \|f\|^2_{L^1(B^2)} \right) \\
&\leq\; C\|f\|^2_{L^2(\mathbb{R}^2)}.
\end{aligned}$$

Hence, we Lax–Milgram's Theorem can be applied and (85) has a unique solution. It remains to prove (3). For this, we apply the Fourier transform with respect to the in–plane variables x onto (85). We get an ODE for $\mathcal{F}(U_{ac})$ in terms of z with the Fourier variable ξ as parameter:

$$\frac{\partial^2}{\partial z^2}\mathcal{F}(U_{ac})(\xi,\cdot) - |\xi|^2 \mathcal{F}(U_{ac})(\xi,\cdot) = 0 \qquad \text{for } z \neq 0. \tag{87}$$

We have the following jump conditions at $z = 0$:

$$[\mathcal{F}(U_{ac})(\xi,\cdot)] = 0,\; \left[\frac{\partial}{\partial z}\mathcal{F}(U_{ac})(\xi,\cdot)\right] = -\mathcal{F}(\nabla \cdot m\, \mathbb{1}_{B^2})(\xi) \qquad \text{for } z = 0. \tag{88}$$

The explicit solution of (87)–(88) is given by

$$\mathcal{F}(U_{ac})(\xi, z) = \frac{1}{2|\xi|} e^{-|\xi||z|} \mathcal{F}(\nabla \cdot m\, \mathbb{1}_{B^2})(\xi), \qquad \text{for } \xi \neq 0, z \in \mathbb{R}.$$

Plancherel's identity then yields

$$\begin{aligned}
\int_{\mathbb{R}^3} |\nabla U_{ac}|^2\, dxdz &= \int_{\mathbb{R}^2} \int_{\mathbb{R}} \left(|\xi|^2 |\mathcal{F}(U_{ac})(\xi,z)|^2 + \left| \frac{\partial \mathcal{F}(U_{ac})(\xi,z)}{\partial z} \right|^2 \right) d\xi dz \\
&= \frac{1}{2} \int_{\mathbb{R}^2} \int_{\mathbb{R}} e^{-2|\xi||z|} |\mathcal{F}(\nabla \cdot m\, \mathbb{1}_{B^2})(\xi)|^2\, d\xi dz \\
&= \frac{1}{2} \int_{\mathbb{R}^2} \frac{1}{|\xi|} |\mathcal{F}(\nabla \cdot m\, \mathbb{1}_{B^2})(\xi)|^2\, d\xi.
\end{aligned}$$

□

References

[1] Giovanni Alberti, Guy Bouchitté, and Pierre Seppecher. Phase transition with the line-tension effect. *Arch. Rational Mech. Anal.*, 144(1):1–46, 1998.

[2] Fabrice Bethuel, Haïm Brezis, and Frédéric Hélein. *Ginzburg-Landau vortices*. Progress in Nonlinear Differential Equations and their Applications, 13. Birkhäuser Boston Inc., Boston, MA, 1994.

[3] Antonio Capella, Christof Melcher, and Felix Otto. Wave-type dynamics in ferromagnetic thin films and the motion of Néel walls. *Nonlinearity*, 20(11):2519–2537, 2007.

[4] G. Carbou. Thin layers in micromagnetism. *Math. Models Methods Appl. Sci.*, 11(9):1529–1546, 2001.

[5] Juan Dávila and Radu Ignat. Lifting of BV functions with values in S^1. *C. R. Math. Acad. Sci. Paris*, 337(3):159–164, 2003.

[6] Antonio DeSimone, Hans Knüpfer, and Felix Otto. 2-d stability of the Néel wall. *Calc. Var. Partial Differential Equations*, 27(2):233–253, 2006.

[7] Antonio Desimone, Robert V. Kohn, Stefan Müller, and Felix Otto. Repulsive interaction of Néel walls, and the internal length scale of the cross-tie wall. *Multiscale Model. Simul.*, 1(1):57–104 (electronic), 2003.

[8] Antonio DeSimone, Stefan Müller, Robert V. Kohn, and Felix Otto. A compactness result in the gradient theory of phase transitions. *Proc. Roy. Soc. Edinburgh Sect. A*, 131(4):833–844, 2001.

[9] Carlos J. García-Cervera. One-dimensional magnetic domain walls. *European J. Appl. Math.*, 15(4):451–486, 2004.

[10] A. Garroni and S. Müller. Γ-limit of a phase-field model of dislocations. *SIAM J. Math. Anal.*, 36(6):1943–1964 (electronic), 2005.

[11] Alex Hubert and Rudolf Schäfer. *Magnetic domains: The analysis of magnetic microstructures*. Springer–Verlag, 1998.

[12] Radu Ignat. The space $\mathrm{BV}(S^2, S^1)$: minimal connection and optimal lifting. *Ann. Inst. H. Poincaré Anal. Non Linéaire*, 22(3):283–302, 2005.

[13] Radu Ignat. A survey on some new results in ferromagnetic thin-films. In *Séminaire: Équations aux Dérivées Partielles. 2007–2008*, Sémin. Équ. Dériv. Partielles, pages Exp. No. VI, 19. École Polytech., Palaiseau, 2008.

[14] Radu Ignat. A $\gamma-$convergence result for Néel walls in micromagnetics. *Calc. Var. Partial Differential Equations*, 36(2):285–316, 2009.

[15] Radu Ignat and Benoit Merlet. Lower bounds for Bloch walls in micromagnetics. *submitted*.

[16] Radu Ignat and Felix Otto. A compactness result for landau state in thin-film micromagnetics. in preparation.

[17] Radu Ignat and Felix Otto. A compactness result in thin-film micromagnetics and the optimality of the Néel wall. *J. Eur. Math. Soc. (JEMS)*, 10(4):909–956, 2008.

[18] Robert V. Kohn and Valeriy V. Slastikov. Another thin-film limit of micromagnetics. *Arch. Ration. Mech. Anal.*, 178(2):227–245, 2005.

[19] M. Koslowski, A. M. Cuitiño, and M. Ortiz. A phase-field theory of dislocation dynamics, strain hardening and hysteresis in ductile single crystals. *J. Mech. Phys. Solids*, 50(12):2597–2635, 2002.

[20] Matthias Kurzke. Boundary vortices in thin magnetic films. *Calc. Var. Partial Differential Equations*, 26(1):1–28, 2006.

[21] Christof Melcher. Micromagnetic treatment of Néel walls. *Arch. Rat. Mech.*, 168:83–113, 2003.

[22] Christof Melcher. Logarithmic lower bounds for Néel walls. *Calc. Var. Partial Differential Equations*, 21(2):209–219, 2004.

[23] Roger Moser. Ginzburg-Landau vortices for thin ferromagnetic films. *AMRX Appl. Math. Res. Express*, 1:1–32, 2003.

[24] C. B. Muratov and V. V. Osipov. Theory of 360[degree] domain walls in thin ferromagnetic films. *Journal of Applied Physics*, 104(5):053908, 2008.

[25] Frank Pacard and Tristan Rivière. *Linear and nonlinear aspects of vortices.* Progress in Nonlinear Differential Equations and their Applications, 39. Birkhäuser Boston Inc., Boston, MA, 2000. The Ginzburg-Landau model.

[26] Tristan Rivière and Sylvia Serfaty. Limiting domain wall energy for a problem related to micromagnetics. *Comm. Pure Appl. Math.*, 54(3):294–338, 2001.

[27] Tristan Rivière and Sylvia Serfaty. Compactness, kinetic formulation, and entropies for a problem related to micromagnetics. *Comm. Partial Differential Equations*, 28(1-2):249–269, 2003.

[28] Michael Struwe. *Variational methods*, volume 34 of *Ergebnisse der Mathematik und ihrer Grenzgebiete. 3. Folge. A Series of Modern Surveys in Mathematics [Results in Mathematics and Related Areas. 3rd Series. A Series of Modern Surveys in Mathematics]*. Springer-Verlag, Berlin, fourth edition, 2008. Applications to nonlinear partial differential equations and Hamiltonian systems.